Aus der Poliklinik für Zahnerhaltung und Parodontologie

der Ludwig-Maximilians-Universität München

Direktor: Prof. Dr. Reinhard Hickel

**MICRO-COMPUTED TOMOGRAPHY IN CARIES RESEARCH**

Dissertation

zum Erwerb des Doktorgrades der Zahnheilkunde

an der Medizinischen Fakultät der

Ludwig-Maximilians-Universität zu München

Vorgelegt von

*TATIANA NOGUEIRA ROCHA CLEMENTINO LUEDEMANN*

aus

Brasília, Brasilien

2007

Mit Genehmigung der medizinischen Fakultät

der Universität München

*To my husband Gustavo and my son João Pedro*

# Table of Contents

**PART II. µCT vs. TMR:  A VALIDATION STUDY**

**PART III. MICRO-CT AND DENTIN STUDY: A THREE-DIMENSIONAL**

**EVALUATION OF CARIES**

# Introduction

In cariology research there is an increased demand for non-destructive techniques of mineral change analyses. Not only do they considerably simplify investigative procedures in the laboratory (Hafstrom-Bjorkman *et al.*, 1992), but allow longitudinal experiments to be conducted, once samples are preserved and can be analysed after different procedures in the same study, enabling evaluation of mineral loss, gain and its kinetics (Dowker *et al.*, 1999).

In 1991, ten Bosch & Angmar-Månsson in a detailed review of quantitative methods for mineral changes analysis recommended the development of a radiographic method to quantify mineral loss from whole teeth (ten Bosch and Angmar-Mansson, 1991). The interest in radiation techniques is due to the ability of x-ray to travel through matter (Bonse and Busch, 1996; Herkstroter *et al.*, 1990), for non-destructive evaluation and testing of objects (Zolfaghari, 1996).

In conventional radiography, X-rays pass through the investigated object, and the transmitted intensity is recorded as a two-dimensional image. The information contained in this radiograph is a projection of the absorption density in the sample onto the plane perpendicular to the X-ray beam direction. If now the sample is imaged several times in different orientations, three-dimensional (volume) information on the sample structure can be obtained using computer algorithms. This is called a tomographic reconstruction or tomography. It enables one to look at slices of the investigated object without physically cutting it.

The first report on x-ray microtomography (micro-CT) was published in 1954 (Lindblom, 1954), and since than this method is used in different areas of science, like bone investigation,

mineralogy, biology, material sciences, engineering sciences, paleobiology and others (Elhila *et al.*, 1996; Kalukin *et al.*, 2000; Rossi *et al.*, 2004). At the end of the 80's the first research on micro-CT was published in the dental field, but only in the last few years it is gaining importance in dental research.

Micro-CT is a variation of x-ray attenuation methods, which has been used to study demineralized lesions. Attenuation means the graduate diminution of radiation flux through a particular feature due to the process of scattering and absorption of the radiation. In both processes, the X-ray photon interacts with the atoms of the material. In scattering, the X-ray photon continues with a change in direction with or without a loss in energy. In absorption, the energy of the X-ray photon is completely transferred to the atoms of the material. The fundamental law of attenuation, also called, Beer-Bouguer-Lambert law, states that the attenuation process is linear in the intensity of radiation and amount of matter, provided that the physical state (i.e., composition) is held constant. The attenuation coefficient is an inherent property, dependent on the atomic number of the object, its density and on the intensity of the X-ray energy, thus allowing quantitative classifications to be made (Davis and Wong, 1996a).

Micro-CT is derived from the Computed Axial Tomography (CAT), but mostly applied for laboratory purpose, which makes your use possible in higher order of energy and finer resolution. It is a non-destructive technique, which allows high spatial resolution of inner structures to be recorded (Anderson *et al.*, 1996; Rhodes *et al.*, 1999; Stock *et al.*, 2002). Depending on the x-ray source and the scanner design, the linear resolution for micro-CT is about 2-100 μm (Wong *et al.*, 2000). The data can be registered both in two or three dimensions and used for qualitative or quantitative analyses (Dowker *et al.*, 1997; Mercer *et al.*, 2003; Oi *et al.*, 2004; Peters *et al.*, 2003; Rhodes *et al.*, 1999; Rhodes *et al.*, 2000).

The current work has been divided into three parts: *I. X-ray Micro-Computed Tomography: Basic Concepts, II. Validation of micro-CT for Enamel Caries Research* and *III. Micro-CT and Dentin Study: A Three-Dimensional Evaluation of Caries*. The first part includes an introduction to the basic concepts of X-ray micro-computed tomography (chapter 1). A chronological review of micro-CT in the present caries research is pointed out in the second chapter. In chapter 3 we evaluate a commercial micro-CT equipment and discuss its feasibility to measure quantitatively the mineral content of whole tooth and the relevant conditions related to the limitation of the system.

In the second part we applied X-ray micro-CT to the study of the natural enamel caries lesion. As an important step for the validation of the method, a correlation was determined between the new technology and a gold-standard. Transverse microradiography (TMR) was the elected method for this study because it is the analytical method which yields the most detailed quantitative information of mineral content, mineral changes, and mineral distributions of tooth samples (Arends and ten Bosch, 1992).

A practical application of the method for three-dimensional studies is related on the third part. The ability of a prototype enzymatic solution to remove dentin caries was for the first time evaluated. A mathematical model was used to access the thickness of the remained demineralized tissue and threshold image analysis was applied for the determination of the volume of removed carious tissue.

# Part I

# X-ray Micro-computed Tomography:

# Basic Concepts

# Chapter 1

# X-ray Micro-computed Tomography

## 1.1 Introduction

After the x-ray computed tomography invention, in 1972, by Hounsfield and Cormark, the diagnostic medicine has gained in resolution, accuracy and speed, once images of internal features, based on x-ray attenuation coefficients, became feasible.

Micro-CT is a miniature sort of the original clinical CAT scanners. Two main technical differences between both make it possible to obtain a much better resolution. First, the different projections in medical computer tomography are made by rotating the X-ray source and detector around the object (patient), causing mechanical vibrations. For the study of materials, it is possible to rotate the object, thereby reducing the vibration and enhancing the resolution. The second difference is the size of the X-ray source which is 5-10 $\mu$m in micro-focus computer tomography compared with a millimetre in medical applications. The smaller source increases the sharpness of the projection by reducing the penumbra (Figure 1). This makes it possible to put the object near the X-ray-source and to increase the primary enlargement of the object, which again enhances the resolution (Van Geet, 1997)
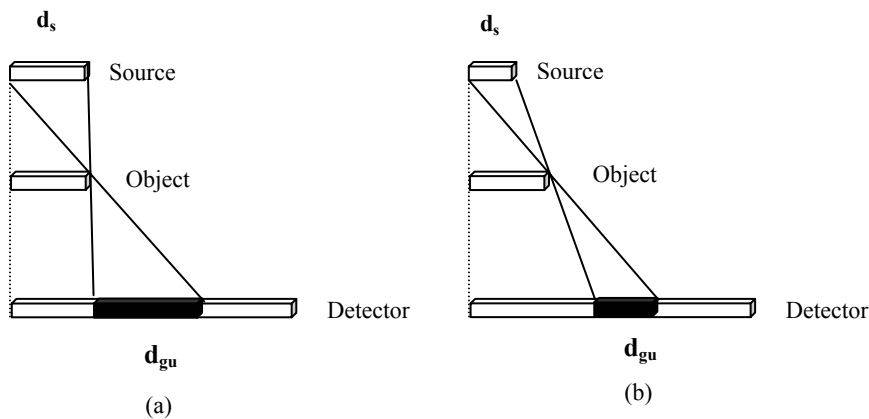
**Figure 1.** $D_{gu}$ Geometrical unsharpness; $d_s$ focal spot size (Van Geet, 1997).

## 1.2 Principles

The simplest common elements of X-ray radiography are an X-ray source, an object to be imaged through which the X-rays pass, and a series of detectors that measure the extent to which the X-ray signal has been attenuated by the object (Ketcham and Carlson, 2001). The principle of absorption micro-CT consists in reconstructing the linear attenuation coefficient, within an object, from measurements of the attenuation of an x-ray beam passing through the sample at different viewing angles (Anderson *et al.*, 1996; Salome *et al.*, 1999). Each element of the projection is a line integral of the linear attenuation coefficient in the sample along the x-ray beam path (Salome *et al.*, 1999). A map of the linear attenuation coefficient can then be recovered from these line integrals using suitable reconstruction algorithms (Bonse and Busch, 1996; Kak and Slaney, 1988).

For quantitative absorption measurements it is necessary to determine the intensity with and without the object. As, in a real experiment, the profile of the incoming beam is not perfectly

uniform (neither in the direction perpendicular nor in the one parallel to the beam) and as it varies slowly with time, it is important to take both images within a few minutes and without moving the detector (i.e. the incoming intensity is determined by moving the object out of the beam path) (Wolfgang, 2001).

Linear attenuation (or extinction) coefficient ($\mu$) is a monochromatic weight, related to the attenuation of the radiation, associated to a monochromatic bundle, in the context of the Beer-Bouguer-Lambert law (Figure 2). In case of no scattering, it is referred as linear absorption coefficient and, in case of no absorption, it is so-called linear scattering coefficient (Sokolik, 2005). Basically, the law states that absorbance is proportional to the concentration of radiation-absorbing molecules in the sample.
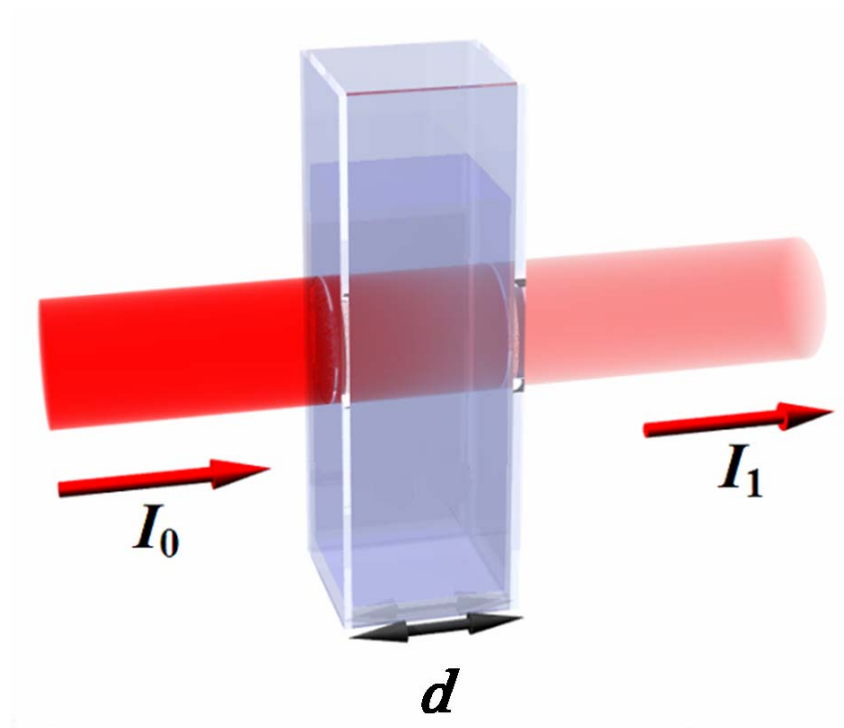


**Figure 2.** Diagram of Beer-Lambert absorption of a beam of light as it travels through a cuvette of size $d$.

Thus, the linear attenuation coefficient (μ) is the probability that an X-ray or gamma-ray photon will interact with the material it is traversing, per unit path length travelled. It is usually reported in units of $cm^{-1}$ and depends on the photon energy, chemical composition and physical density of the material. For monoenergetic X-rays, the fraction of incident X-rays expected to penetrate through a thickness $d$ without interacting with the material is:

$$\frac{I}{I_0} = e^{-\mu d} \tag{1}$$

Another way to express the linear attenuation coefficient is by the mass attenuation coefficient (MAC) $[cm^2/g]$ multiplied by the density $\rho$ $[g/cm^3]$ (2).

$$\mu = MAC \times \rho = \frac{\mu}{\rho} \times \rho \tag{2}$$

The advantage of expressing the linear attenuation coefficient in this way is that the mass attenuation coefficient is independent of density and can be computed from the mass attenuation coefficients of the constituent elements. For any material, the mass attenuation coefficient ($\mu_{mass}$) is a weighted sum of the mass attenuation coefficients of the component elements.

$$\mu_{mass} = a\mu_1 + b\mu_2 + c\mu_3 \dots x\mu_n \quad [cm^2/g] \tag{3}$$

Differences in linear attenuation coefficients among tissues are responsible for X-ray image contrast. In computed tomography (CT), the function imaged is in fact the distribution of linear attenuation coefficients (Figure 3).
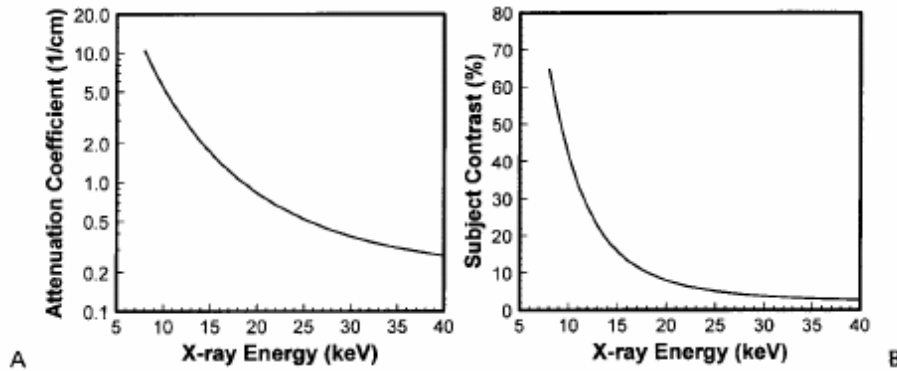
**Figure 3.** *A:* The value of the linear attenuation coefficient increases as the x-ray energy decreases. *B:* The subject contrast is shown as a function of the x-ray energy. Lowering the x-ray energy, increases the value of μ, this increases the subject contrast of the sample (Bushberg, 1994).

## 1.3 X-ray Source

In X-ray tubes, X-rays are generated by stopping fast electrons in a target material inside an evacuated glass tube. The energy of the X-ray photons is of the order of the electron energy. The electrons' acceleration voltage determines the upper limit of emitted X-ray energy. X-rays produced by this principle are called Bremsstrahlung with a white continuum spectrum (Bonse and Busch, 1996).

Three variables concern with effectiveness of the x-ray source: focus-size, energy spectrum and intensity. The focus-size is very closely related with the linear resolution of the micro-CT. One can find equipments with dual spot-size. A smaller, which allows more details to be recorded, but at a cost of intensity, and a larger, which can be used intending to improve counting statistics with a little cost in linear resolution. The energy spectrum is related with the penetrability of an X-ray. Higher energy penetrates more efficiently, but can be less sensitive to changes in material density and composition. The energy spectrum generated is usually described in terms of the peak X-ray energy (kVp), but actually consists of a

continuum in which the level with maximum intensity is typically less than half of the peak (keV). The X-ray intensity directly affects the signal-to-noise ratio and thus image clarity. Higher intensities improve the underlying counting statistics, but often require a larger focal spot (Ketcham and Carlson, 2001).

## 1.4 Detectors

After passing through the object, the X-rays are detected by a detector system, which should detect every incident photon of the complete band of X-ray energies (efficiency, spectral sensitivity), its response should be linear over a large range of intensities (linearity, dynamic range) and the detector's spatial resolution should match that of the source (spatial resolution).

Presently, charge-couple device (CCD) cameras are mostly applied in micro-CT set up. Due to its sensitivity to visible light and to prevent damage by the radiation, CCD cameras are mostly used with a scintillator. To obtain a quantitative signal in digital form the optical image is projected by a lens system to a CCD chip where the light is converted to an electrical signal for each picture element by means of an analogue digital converter (ADC) and stored to computer disk memory for further evaluation. Scintillation screens currently limit the spatial-resolution capability of tomographic systems. (Bonse and Busch, 1996).

## 1.5 Systems

The first micro-tomographic image of a hard tissue specimen, in this case the shell of biophalaria glabrata (a snail), with a resolution of 12 μm, was produced by Elliott and Dover, in 1982. In the period following, a lot of systems have been developed (Davis and Wong, 1996a). Until this time one can find four different types of micro-CT.

The first generation of micro-CT, or the so called, point scanning or single detector system (Figure 4) is composed of an x-ray source, which emanates parallel geometrical beams, collimator and one single detector. It is the simplest arrangement for the micro -CT technology.

Pinhole
collimator

Specimen
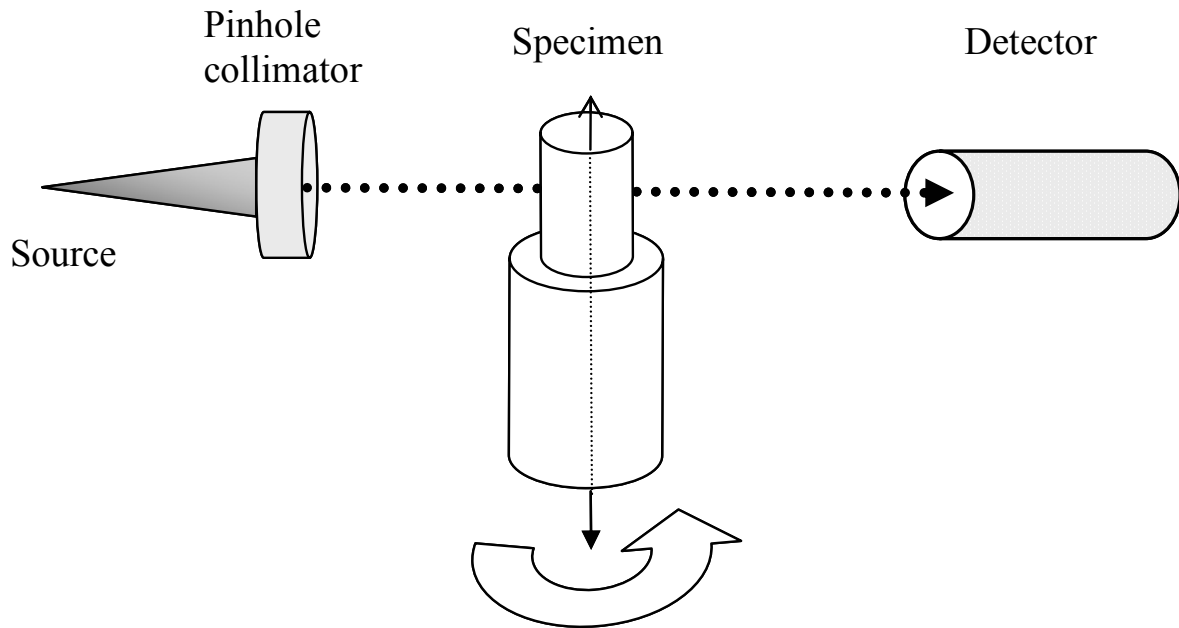
Detector

Source

**Figure 4.** Schematic image of a point-scan system.

In order to obtain the absorption index map of at least a single cross section of the sample, a one-dimensional (1D) scanning of the sample or the coupled source-detector unit must be performed. The scanning direction (x-axis) is perpendicular to the beam (y-axis) and the axis of rotation (z-axis) and, in order to investigate a 3D sample volume, it requires additional scanning along z-direction (rotation axis) (Bonse and Busch, 1996).

For reconstruction of 3D images from parallel projection, filtered back-projection algorithm has been currently used. It has been shown to be extremely accurate and amenable to fast implementation and will be derived by using the Fourier Slice Theorem. This theorem is

brought into play by rewriting the inverse Fourier transform in polar coordinates and rearranging the limits of the integration therein (Kak and Slaney, 1988).

The advantages of point scanning apparatus are: (a) its reasonable price, comparing with the next versions; (b) the possibility of using energy detector resolving, which allows monocromatization of radiation, avoiding beam-hardening artefacts (see later) (Bonse and Busch, 1996; Wong *et al.*, 2000). Thus, the local mass concentration can be determined from the measured linear attenuation coefficient, when the composition is known (Davis and Wong, 1996a; Wong *et al.*, 2000). Wong et al. (Wong *et al.*, 1995) showed that the system was sufficiently sensitive to detect an increase in the mean cross-sectional mineral concentration of ~ 1.3 to ~ 1.5 $g/cm^3$ from the distal metaphysic to the proximal end of the femur, respectively. (c) The lack of blurring effects caused by scattering (Davis and Wong, 1996a), because detection of scattered radiation can easily be made negligible by an appropriate collimator arrangement (Endo *et al.*, 2001). In this sense, contribution of scattered radiation to the detector signal can, with good collimation, be <1% (Carlsson, 1999). (d) All pixels are generated from signals from the same detector, which means that detector artefacts, as ring artefacts are avoided (Carlsson, 1999).

Disadvantages would be: (a) the long time required for scanning (Anderson *et al.*, 1996), (b) it is not useful, if high resolution is necessary, because by reducing of aperture diameter and use of smaller step sizes, one consequently looses of intensity, too (Bonse and Busch, 1996). However, according to Carlsson, C.A. (1999), a detector can be large enough to get maximal efficiency (Carlsson, 1999). Also, the capabilities of their first generation system constrained practicable measurement to a small number of slices through lesions formed in cut blocks with a 2 x 2.5 $mm^2$ cross-section.

The next micro-CT, which seems more similar with the third generation of CAT scanner, has fan-beam geometry (Figure 5). That means, a point source of radiation emanates a fan-shaped beam and, on the other side of the object, a bank of detectors is used to make all the measurements in one fan simultaneously (Kak and Slaney, 1988). It is also called a linear-array system. In it, the whole slice can be projected and registered at the same time, through a linear array of detector elements, resulting in an expeditious reconstruction of data. For 3D examination, it has to be performed a time consuming slice-by-slice examination of the object. One other disadvantage is the waste of most photons, during exposure, on the collimator, resulting in inefficiency in terms of data acquisition (Axelsson and Danielsson, 1994).
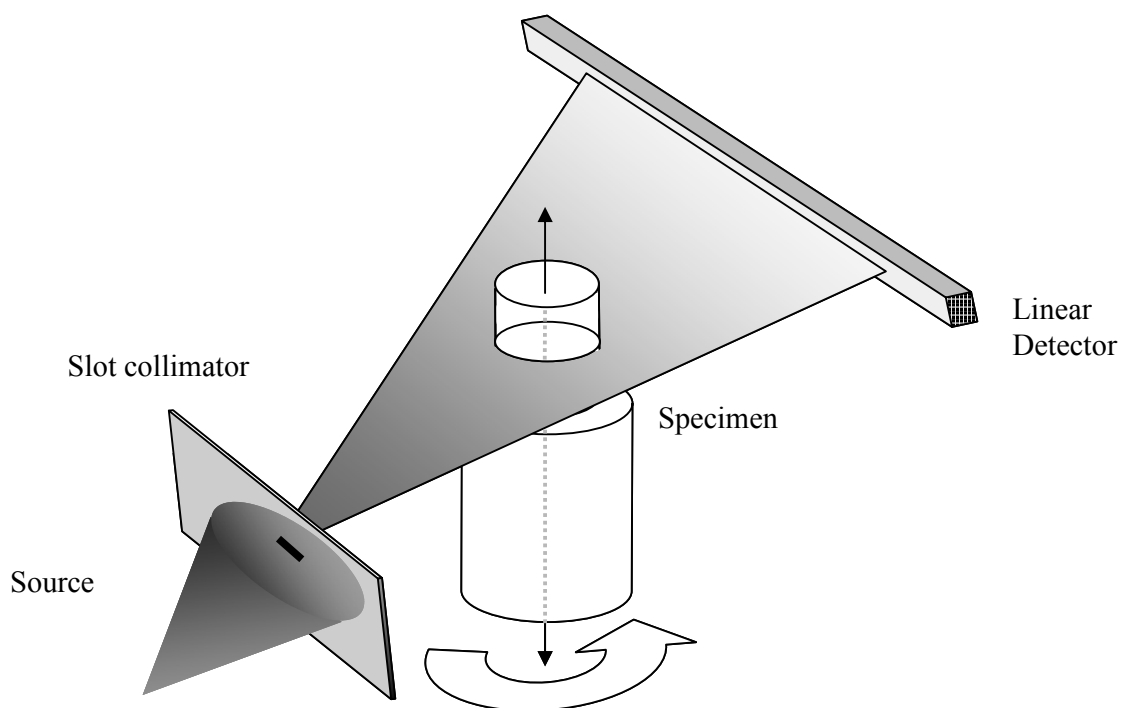


**Figure 5.** Schematic image of a fan-mean system.

For fan-beam geometry, the reconstruction of data gains a little in complexity, because the back-projection now has to be weighted. Davis (Davis, 1998) had developed a faster tomographic fan-beam back-projection, which takes half of time comparing to the

conventional fan beam back projection algorithm, without sacrificing accuracy. According to Davis & Elliott (Davis and Wong, 1996a), there are no advantages of this system over the next one to be presented. This geometry is used in the µCT 20 (SCANCO Medical AG, Bassersdorf, Switzerland) that will be studied in the chapter 4 of the current work.

The cone beam system, which is categorized as the third generation of micro-CTs, uses a cone formed source and a 2D detector. Such systems allow complete three-dimensional images to be obtained without the need for scanning each slice individually (Davis and Elliott, 1997), so that the complete sample can be radiated at once (Figure 6). An practical example of this geometry is shown in chapter 6 (µCT 40; SCANCO Medical AG, Bassersdorf, Switzerland).

Also called area-array system or cone-beam CT, it demands more sophisticated algorithms to reconstruct the image, due to the enhanced polychromatic characteristic of the beams, which leads to beam hardening effects. Nevertheless, the use of sources with small focus size, which diminishes the cone area, leads to less significant errors in reconstruction of the images, when specimen size is small compared to its distance to the x-ray source (Davis and Elliott, 1997).



**Figure 6.** Schematic picture of a cone-beam system

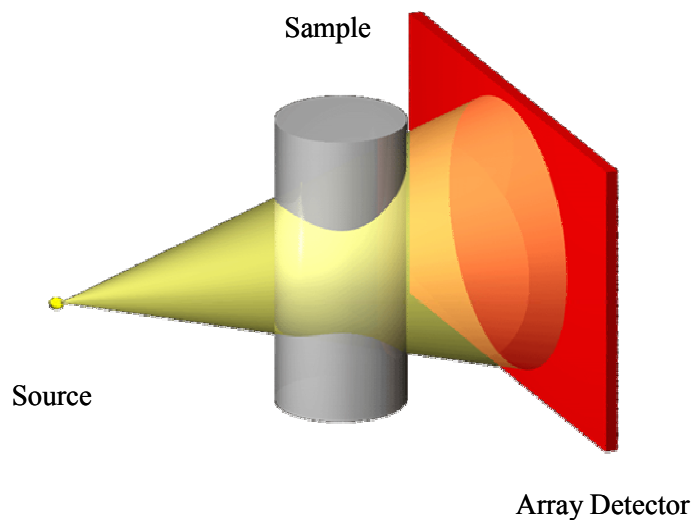It is well known that most material preferentially absorbs low energy x-rays photons more than high-energy (Hsieh *et al.*, 2000). Beam hardening is the phenomenon that a polychromatic X-ray beam becomes more penetrating, or harder, as it traverses through matter. The X-ray beams used in medical imaging are polychromatic with a moderately broad energy spectrum. The attenuation processes in matter are energy dependent. Non-uniform attenuation of different energies results in the preferential depletion of X-rays in energy ranges with higher attenuation coefficients. In general, X-rays in energy ranges that are more easily attenuated are referred to as soft X-rays while those in ranges that are more penetrating are referred to as hard X-rays. Thus, beam hardening is the process of selective removal of soft X-rays from the X-ray beam. As these X-rays are removed, the remaining beams are progressively harder or more penetrating. The amount of beam hardening depends on the initial X-ray spectrum as well as on the composition of the material or tissue traversed. However, for any fixed initial X-ray spectrum and tissue type, the process of beam hardening represents a monotonic increase in beam hardness as a function of tissue thickness traversed (Pettersson *et al.*, 1998).

As a result of beam hardening, the effective attenuation coefficient of a material depends on the thickness of material traversed. This effect causes so-called beam hardening artefacts in CT images. If uncorrected, beam hardening artefacts appear as cupping, or a reduction of the reconstructed attenuation coefficient toward the centre of a large object (Pettersson *et al.*, 1998). According to Dowker et al. (Dowker *et al.*, 2003) this phenomenon could be minimised by careful calibration.

According to Endo et al. (Endo *et al.*, 2001), its major disadvantage is the scattered radiation, which can not be avoided and may enhance the noise in reconstructed images, and thus affect

low-contrast detect ability. Nevertheless, the use of a crystal collimator between the sample and the detector can significantly depress this factor (Takeda *et al.*, 1994).

The fourth generation of micro-CT was built to overcome the problems with ring artefacts, common in the cone-beam scanners. A ring artefact is a phenomenon which occurs whenever a 'curve' with sharp edges is subject to Fourier analysis. Representation of the profiles measured with a limited number of Fourier harmonics is imperfect, resulting in high-frequency oscillations at the edges, and the image can therefore exhibit some noticeable spatial signal intensity variations at intensity boundaries: the Gibbs phenomenon, overshoot artefacts or "ringing" (Davis and Elliott, 1997). The artefacts can be suppressed by filtering the images. However, filtering can in turn reduce spatial resolution (Pettersson *et al.*, 1998).

This new system employees the method of time delay integration (TDI), which is a technique originally designed for increasing the allowable exposure (or integration) time (and hence signal-to-noise ratio) in the acquisition of linearly moving images. TDI uses a two-dimensional CCD which is scanned in such a way, synchronised with the movement of the specimen, so as not to introduce motion blurring (Davis and Elliott, 1997). According to Dowker et al. (Dowker *et al.*, 1997), an advantage of this system is that the sensitivity of each pixel within a single vertical column of the scanned image is identical, so that only one calibration per column, rather than per pixel is necessary (Davis and Elliott, 1997; Dowker *et al.*, 1997). A physical description for the construction of this system is found in Davis & Elliott (Davis and Wong, 1996a). According to them, the use of TDI scanning in microtomography will also have the advantages of improving the accuracy with which features in the specimen can be quantified and enabling to scan specimens which are larger than the CCD imaging area or the X-ray beam. This latter feature would be of particular significance when using a synchrotron source (Davis and Elliott, 1997). Also, high spatial

resolution (5 μm), high dynamic range and high signal-to-noise ratio are here present, which results in high contrast resolution and excellent discrimination of very small differences in attenuation coefficient (< 1% depending on the specimen). The disadvantage of this system is the greater complexity in constructing the equipment and the necessity of longer exposure time.

## 1.6 Synchrotron Radiation (SR)

A revolution in micro-CT images, according to resolution and quality of image was achieved after the use of synchrotron sources. Synchrotron radiation refers to the electromagnetic radiation emitted by ultra relativistic electrons (energies of several GeV), circulating in storage rings, where they are accelerated by a magnetic field (Cloetens et al., 2001). Its large flux of photons and better collimation provides more x-rays per unit area on the sample, allowing for better spatial resolution (Dowker et al., 2003; Landis et al.), which can be near to 1 μm (Bonse and Busch, 1996). The higher flux and continuous spectrum allow researchers to choose a monochromatic beam with a small band pass, which greatly improves the sensitivity of microtomography to smaller x-ray absorption variations within the sample. The high degree of monochromaticity also mitigates the problem of beam hardening (Cloetens and Baruchel, 2002; Landis et al., ; Spanne, 1989). According to Davis and Wong (Davis and Wong, 1996a), SR can be used in all categories of microcomputed tomographic equipment.

The advantages of synchrotron radiation (SR) over X-rays from X-rays tubes are: high intensity (Cloetens et al., 2001; Morton et al., 1990) and/or brilliance, collimation, tuneability over a wide wavelength spectrum (infra-red through visible and ultra-violet), linear or elliptical polarized radiation (Bonse and Busch, 1996). The beam energy can be tuned over a broad range, allowing the optimum x-ray absorption to be chosen for each sample, depending

on size and/or composition. Thus it is possible to construct compositional maps of objects (Landis *et al.*, ; Spanne, 1989).

According to Morton et al. (Nuzzo *et al.*, 2002) the use of SR micro-CT as compared with standard micro-CT offers the opportunity of an accurate investigation of local bone mineral content in addition to microarchitectural analysis. Moreover, the use of a high resolution CCD based two-dimensional detector allows the finer spatial resolution of x-ray microtomography to be realized, while keeping the sample scanning time to a minimum (Landis *et al.*). However, at the current time, one can find difficulties to work with SR due to its high cost and sample size limitations (Dowker *et al.*, 2003). Specimens can not be larger than few millimetres.

# Chapter 2

# Micro-CT in Caries Research

## 2.1 A Chronological Review

The use of microtomographic technique in dentistry dates only two decades. The method is thus new and has to be tested and discussed. In this field, a few numbers of schools have been giving effort, testing the technology, contributing to enhancement of physical properties, as resolution and reduction of artefacts, implementation of image analysis techniques to achieve common purposes as the higher quality, sensitivity and accuracy of the results.

One of the most expressive potential of the micro-CT for dentistry is for evaluation of mineral content and changes in dental hard tissue. As the results from scanning procedures are expressed as attenuation coefficient, the equivalence of this value to mineral content should be known, after a prudent calibration.

However quantification of mineral changes have started in early 90's, when Gao et al. (Gao *et al.*, 1993) used tomographic technique, together with microradiography, to the study of mineral distribution in tooth rods before and after demineralization, and after remineralization. In this experiment, first generation tomographic equipment was used with 10 μm linear resolutions to scan physically cut teeth (2 x 2.5 mm$^2$ cross-sections).

Demineralization results throughout the depth of the lesion showed good agreement with earlier results. According to the authors, micro-CT can give new insights into the process of remineralization of early carious lesions. As suggestion from the authors, micro-CT should also be used in investigations of chemical reaction, including those at extremes of temperature, in which the microscopic spatial distribution of the x-ray absorption changes on the timescale of a few minutes or to a few weeks.

Anderson et al. (Anderson *et al.*, 1996) compared the mineral content of enamel and dentine in human premolar rods (2 x 2.5 mm$^2$) and enamel pearls, using a first generation microtomographic apparatus at 40 kV and 2 mA. The system was periodically calibrated with a flux-grown crystal of fluorapatite, whose linear absorption coefficient could be calculated from its density, chemical composition and published elemental-mass absorption coefficients. It insured that systematic errors in the determined linear absorption coefficient were minimized. Aluminium wire was also used in some slices to check the measured linear absorption coefficient. Analysing selected regions of interest, Anderson et al. (Anderson *et al.*, 1996) also showed agreement of mineral distribution in the premolars with earlier microradiographic studies and density measurements. For the pearl of enamel the findings were again consistent with earlier results. Interestingly, however, is the finding on the mineral gradient in dentin slices, which were higher at deeper dentin than in the dentin close to the amelo-dentinal junction. As the porous volume and water content at deeper dentin increases in comparison to the superficial dentin (Garberoglio and Brannstrom, 1976; Pashley *et al.*, 1991), one could expect a lower linear attenuation coefficient of the inner part, as showed by Wakabayashi et al, in 2005 (Wakabayashi *et al.*, 2005)

In 2000, Wong & Elliott (Wong *et al.*, 2000) quantified the mineral concentration and its gradient by studying the pattern of mineralization in rat incisors. In this study, measurements

of mean linear absorption coefficient for enamel from micro-CT slices were determined. A first generation AgKα micro-CT, with 10 µm Pt aperture was used. An energy dispersive Si (Li) detector was used, connected to two single channel analysers, in parallel, one with a narrow (for calibration) and the other with a wide electronic energy window, to maintain effective monochromatism for the images reconstructed with the higher count rate wide window. To facilitate separation of enamel to dentin (boundaries), projections with 640 points were generated by linear interpolation and back-projected onto a 640 x 640 grid. Each incisor was mounted so that the axis that most closely followed the length of them coincided with the rotation axis of the micro-CT. Internal calibration was provided by a 0.5 mm diameter pure aluminium wire attached by varnish alongside the incisor. The data collection time was about 18 h for each slice. The boundary was established by drawing a polygon at the amelodentinal junction (ADJ) and external enamel surface. At similar linear absorption coefficient (LAC), between enamel and dentin, the ADJ was approximated by using adjacent slices as reference. Within the polygon, all the pixels, above 3 cm$^{-1}$, were set to 1 (enamel boundary), and the rest to 0. The only region where it could happen of lower value for enamel was along the edges. This was reduced by resetting all the 1 pixels, adjacent to the 0 pixel, to 0 to create a new binary image. This procedure was then repeated and the final image was used as a mask to select enamel pixels for the determination of the mean and distribution of the LACs. Also, isodensity surfaces were computer generated in this study. According to them, micro-CT has the advantage to be used in different studies of mineral pattern, without necessity of stains.

In 2001 a quantitative study of the effect of pumicing and etching on the remineralization of enamel opacities was made by Peariasamy et al. (Pearisamy and Anderson, 2000). The method included micro-CT, contact microradiography (CMR) and infrared reflectance. For the micro-CT study, a linear resolution of 15-30 µm was achieved in cut specimens of 2.0 x 2.0 mm cross section. Also here, aluminium wire was used to check the system. The results

from micro-CT showed similarity with the ones from CMR and the formation of surface was visible for the treated regions.

The first experiment conducted in whole teeth was published in 2003. Therefore, a longitudinal study of subsurface enamel lesions during in vitro demineralization was made by Dowker et al. (Dowker *et al.*, 2003). Three third molars were fixed by epoxy putty to a kinematical mount, which could be removed and accurately repositioned on the micro-CT rotation stage. A fourth-generation micro-CT system was operated at 90 kV, 0.26 mA and a 0.5 mm Al filter was employed. Each whole tooth was scanned as a ~3-mm-wide transverse block, requiring 17h, for 15 μm voxel size. Raw data were reconstructed using a cone beam version of the cartesian axes pre-projection algorithm (Davis, 1998). Volume rendering and visualisation of slices were used to control the progress of demineralization. In this study, precise delimitation of the interface tooth/air was not possible due to the contribution of both surfaces for voxels at this area. Superimposition of series of data sets was also variable in few voxels. The results from this study are consistent with previous studies and finding derived from previous microanalysis of calcium and phosphorus concentrations, microradiograms and scanning electron microscopy.

Also in the domain of the small wavelength, the microtomography has been used to study laser ablation. Mercer et al. (Mercer *et al.*, 2003) measured the progression of crater growth during repeated sequential application of a commercial dental Er:YAG laser to human enamel and dentin. Here tooth rods of 2 mm x 2 mm were used, which could be located and relocated onto a rotation axis of the micro-CT scanner. A 1 cm polymethyl-methacrylate jacket with a closed end was placed around the specimen. This assembly could be attached to the upper surface of an aluminium disc, which contained on the underside three balls fixed in an equilateral triangle format. These balls were than, for measurements, located into a three brass

'V' blocks on a mounting plate positioned on the central location axis of the scanner, with accuracy of 0.02 μm in reposition processes. A fourth generation system was set to 50 kV and 1.6 mA with the use of a 2 mm Al filter. Image detector was calibrated using an Al step wedge of known dimensions. Each data set took 10 h to be collected and reconstructions were made with standard filtered fan beam algorithm. The final resolution achieved was of 38.66 μm. Isosurfaces were calculated from complete 3D data sets and a threshold value of mineral concentration was selected at about half the value for that of dentin. This was suggested by Davis and Wong (Davis and Wong, 1996a) for boundary in bones research. They suggested setting a threshold halfway between the attenuation coefficient, or density, of bone and non-bone. All pixels above this threshold are considered to be bone and all below are non-bone. This gives a good approximation to the true bone to non-bone interface when there is a substantial volume of bone adjacent to a large space, but in cases where the trabecular thickness approaches the resolution of the scanner this threshold is too high. However, according to Mercer et al (Mercer *et al.*, 2003), where there is a sharp boundary, like in the case of enamel, dentine and air, this does not present problems. Crater volume measurement, after laser firing, were take through subtraction of voxels, from 3D images. The 2D grey scale sections, which are similar to microradiographs of thinly cut sections, were used for calculation of the depth of the crater. Results from this study confirm previous findings which have used vertical scanning interferometry.

Fearne et al. (Fearne *et al.*, 2004) measured the extent and the distribution of mineral concentration in first permanent molars with idiopathic enamel hypoplasia through an micro-CT experiment. The response of the transmitted X-ray image capture system was pre calibrated with a 10-step aluminium step wedge. Drying artefacts were avoided by maintaining the samples immersed in fluid and, to prevent motion of the specimens, each tooth was located inside a plastic syringe, filled with deionised water, and kept firmly in place

by depressing the plunger lighly in contact with the top of the tooth, before mounted onto the rotation axis of the micro-CT stage. In this study, whole uncut teeth specimens were analysed in terms of mineral concentration with a resolution of 15 μm. Images were available as slice data, similar to the contact microradiography, where mineral profiles could be obtained. Also 3D operations were performed like surface rendering, in which all adjacent voxels with the same mineral concentration are joined by a surface. A reduction of 5% of mineral content could be detected in the affected tooth, compared to the sound control, which could demonstrate the ability of the equipment to distinguish minimal changes in mineralization of enamel tissues.

As the grown interest for biomaterials development reach the research laboratories, sintered hydroxyapatite, as a good compatible representative for bones and teeth, has also gained in importance. Itoh et al. (Itoh *et al.*, 2004) had investigated $CO_3Ap$-collagen sponges with lunge spores, in which osteoblasts can both easily invade and remain. The study was carried out in a microCT device, which worked at 80 kV and 100 μA, to reach a detection of 2 μm as linear resolution. According to the authors, soft x-ray high-resolution micro-CT was successful to construct 3D images of these organic porous sponges.

Microtomographic technique was used also by Hahn et al. (Hahn *et al.*, 2004) to access the effectiveness of chemo-mechanical removal of carious dentin. Ten carious human molars were imaged by an 80 kV and 100 μA micro-CT unit, which offered an average pixel size of 12.4 μm and increments of 26.3 μm, before and after removal procedures. The results of this study showed a dentin statistically less dense after treatment than it was found in sound dentin. On account of this, Hahn et al. brought two concerns to be considerate. One is that there are no established standards for microtomographic density values for caries determination and second, the surfaces, after chemo-mechanical caries removal, are more

irregular than after bur and therefore the density can be lower even tough it could be caries-free, representing a possible limitation of the system for these analyses.

The determination of mineral concentration in deciduous teeth and its pattern was studied by Wong et al. (Wong *et al.*, 2004) through a first generation micro-CT, set at 21.1 keV. Tooth rod of 2 x 2 mm$^2$ was cut and analysed together with a 0.5 mm Al wire. Effective monochromatization was achieved by a setting photon counter in a window range between 4% (narrow) and 40% (wide). The data from the narrow window was used to calibrate the data in the wide window by fitting a 7$^{th}$ order polynomial in order to avoid artefact from polychromatic beams, and to improve signal-to-noise ratio in the final back-projection reconstruction. A binary image was obtained by setting all voxels as described in Wong and Elliott (Wong *et al.*, 2000). LAC values were calibrated using the measured mean LAC of the pure aluminium wire and its published value of 6.87 cm$^{-1}$ at 22.1 keV. Wong et al. have used an aluminium wire to calibrate the detector. In this case, the transformation of data was made assuming that hydroxiapatite as the only content in tooth, with a density of 3.15 g/cm$^3$. LAC (μ) was converted to mineral concentration (C$_e$) by:

$$C_e = \frac{\mu_e \times \mu_{al(pub)}}{\mu_{al} \times \mu_{mhap}} \quad [g/cm^3] \tag{4}$$

Where μ$_e$ is the measure LAC of enamel, μ$_{at(pub)}$ the LAC of aluminium wire for a known energy in keV and μ$_{mhap}$ the mass attenuation coefficient of hidroxiapatite (4.82 cm$^2$/g at 22.1 keV) (Wong *et al.*, 2004). It was confirmed, in this study, the great variance in mineral concentration and gradients between surfaces among deciduous molars from different individuals.

Further work to evaluate the potential of micro-CT in the study of mineral concentration in enamel was published in 2004. Dowker et al. (Dowker *et al.*, 2004) evaluated the ability of a synchrotron source to measure the linear attenuation coefficient of sound and carious enamel. At linear resolution of 1.9 μm, a mapping of mineralization of one single tooth could be done, including analysis and evaluation of the Retzius striaes in enamel. A flux-grown fluorapatite crystal was scanned together with the samples for the standardization of the linear attenuation coefficient. Although uncertainties and variations in the composition of sound and carious enamel limit the accuracy of the determination of mineral concentration from linear attenuation coefficient, results were expressed as $g/cm^3$, for a better comparison of the results with other works. In this study the variation of the results was shown for nine different models of inorganic and organic composition of enamel. Dowker et al. compared the effect of the chosen model upon the parameter derived from linear attenuation coefficient, i.e. mineral concentration or mineral volume fraction. For both parameters, assumptions have to be made and the results showed to have more influence of the model of choice when the linear attenuation coefficient is lower and therefore a greater effect of the organic component is present. Nevertheless, there was a greater uncertainty in the estimation of the mineral volume fraction than the mineral concentration, because not only the chemical composition seems to be the main factor influencing the results, as it is for the determination of mineral concentration, but also the density chosen greatly influenced the results.

# Chapter 3

# Aim of the Study

So far researches have shown a good agreement between micro-computed tomographic results with other methods. However, no direct comparison with a gold standard was ever done. Transverse microradiography has been the most used diagnostic method as gold standard in cariology. Because a direct relationship is provided between radiographic techniques and mineral content, this is a suitable method to be used (Huysmans and Longbottom, 2004). According to Dowker et al. (Dowker *et al.*, 2003) the mineral concentration observed in slices and line profiles extracted from micro-CT volume data sets will always differ from those measured by microradiography in physically cut section of tooth carious enamel. This lack of comparison studies was the concern of this study, which aims to establish a direct correlation coefficient between micro-CT and microradiography, facing the great difference between both methods and with a cost of the ideal measurement condition of the micro-CT. Therefore, TMR prepared slices will be also scanned with a commercial micro-CT equipment in a simulation set up of whole tooth measurements.

The necessity of cutting samples for the TMR analysis and the fact of limiting the representation of the dynamic of the caries lesion to one single micrometric slice provides a

clear necessity to find a method which is not-destructive and enables longitudinal studies to be done. A search for a new gold-standard with these characteristics seems to be essential.

The purpose of this study was:

❖ To evaluate the advantages and limitations of micro-CT for mineral concentration evaluations of sound tooth samples.

❖ To evaluate and correlate the integrated mineral loss and lesion depth of tooth slices with natural caries in enamel by TMR and micro-CT.

❖ To establish a three-dimensional method of evaluation of caries excavation methods

# Chapter 4

# Mineral Concentration of Natural Human Teeth by a Commercial Micro-CT

## 4.1 Abstract

This study aimed to evaluate a commercial micro-CT system (µCT 20) for quantitative analysis of mineral concentration in human enamel and dentin using different methodologies, and thereby compare the obtained results with established data from published literature. A micro-CT device set at 50 kVp (160 µA) was used to scan five whole molars (G1) and five molars ground to 6-mm thickness (G2), as well as to evaluate the mineral concentration of the samples. Mean mineral contents for enamel and dentin were 2.57 (± 0.12) and 1.53 (± 0.12) g/cm$^3$ for G1, and 2.76 (± 0.03) and 1.45 (± 0.02) g/cm$^3$ for G2. Difference between the groups was significant for enamel. For dentin, there was a clear although not significant tendency towards higher values with G1. The equipment could identify and differentiate a higher mineral content of the tooth enamel and dentin from the external to the inner tissue. Further, the absolute mean values of mineral concentration were lower in whole tooth samples than in sectioned samples due to beam hardening. In conclusion, the equipment is well suited for quantifying the mineral content of teeth. However, it is necessary to consider the limited acceleration voltage of the µCT 20 system and to limit sample evaluation to 6-mm thickness.

## 4.2 Introduction

A developing research field in medicine and dentistry is the inspection of specimens by means of non-invasive and non-destructive 3D analytical techniques. These new, innovative techniques boast of a few advantages. First, they do not require the time-consuming preparation of serial sections which means that these new approaches help to save time. Secondly, they do not require specific staining of the object which can affect the organization of the investigated structure. Amongst this array of non-invasive imaging tools, micro-computer tomography (micro-CT) emerges as a potential key tool especially in *in vitro* caries research. This is because it allows image recording of inner structures with high spatial resolution three-dimensionally and without destruction of samples (Lin and Miller, 1996).

Micro-CT is a miniaturized form of CT scanning. It was developed in the beginning of the 1980s predominantly for laboratory purposes on small samples or material experiments, and used frequently in the studies of trabecular bone structure and mineral analysis (Anderson *et al.*, 1996; Davis and Wong, 1996b; Dowker *et al.*, 2004). The principle of absorption of micro-CT consists in reconstructing the linear attenuation coefficient, within an object, from the attenuation measurements of an X-ray beam passing through the sample at different viewing angles. Differences in linear attenuation coefficient among tissues are responsible for X-ray image contrast, which allows quantitative analyses to be made (Davis and Wong, 1996b).

Due to its small size and high X-ray intensity demand, micro-CT is utilized only in laboratorial experiments. Nevertheless, there are new systems of digital volume tomography for dental clinical diagnostics. However, the image quality and resolution of the existing digital dental systems is inferior to that of micro-CT.

To date, commercial micro-CT devices have been used successfully in dental research for qualitative analysis and three-dimensional evaluation of materials as well as in dental treatment procedures (Bergmans *et al.*, 2001; Peters *et al.*, 2003; Sohmura *et al.*, 2004; Wakabayashi *et al.*, 2005). To our knowledge, quantitative evaluation of the mineral concentration (MC) of dental tissues has not yet been investigated on a commercial device.

The aim of this study was to evaluate a commercial micro-CT system for the quantitative analysis of MC at human enamel and dentin using different methodologies, and then compare the obtained results with established data from published literature. In addition, this study tested the null hypothesis that the equipment was sensitive enough to evaluate image data without the need of any specimen preparation, such as the physical cutting of specimens into thin sections. Our second hypothesis was that the equipment was sensitive enough to measure the MCs of enamel and dentin after cutting the samples to 6-mm dentin thickness which according to a published report was the critical thickness for radiographic evaluations at an acceleration voltage of 32 keV (Dowker *et al.*, 2003).

## 4.3 Materials and Methods

A total of 10 extracted third molars, extracted for orthodontic reasons, were selected from a pool of teeth stored in thymol 0.1%. They were divided into two experimental groups: G1 (five whole permanent molars) and G2 (five permanent molars which were cut and ground to 6-mm dentin thickness (Leco VP100, LECO, Kirchheim, Germany). Enamel tissue from vestibular and buccal sides was equally eliminated to reduce the very dense areas and to allow better X-ray absorption through the samples.

## *4.3.1 X-ray microtomography system*

A commercial polychromatic fan-beam microtomographic system (µCT 20, SCANCO Medical AG, Bassersdorf, Switzerland) (Figure 7), with a spot size of 7 µm and a tungsten target using an acceleration voltage of 50 kVp (160 µA), was used. According to the manufacturer, this energy was sufficient to penetrate objects up to 17 mm in diameter. A 0.3-mm aluminum filter was installed in the beam path to cut off the softest X-rays, so as to achieve a detector response close to 32 keV. This was necessary so as to increase the accuracy of the beam hardening correction, because in contrast to synchrotron illumination, the use of polychromatic X-rays creates a problem of beam hardening.
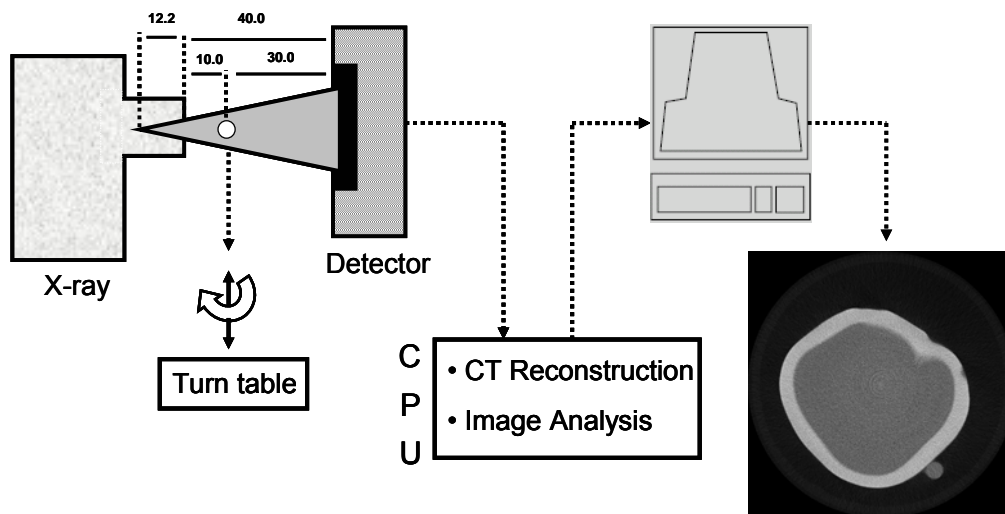


**Figure 7.** Schematic picture for the geometry of the fan bean radiation system and the distances between the X-ray beam and its collimation (12.2 cm); from the last to the sample (10.0 cm) and from the sample to the detector (30.0 cm). The scanner on the left side sends the raw information to the computer, where the data will be reconstructed and images will be analysed.

The object was mounted on a computer-controlled turntable, which synchronized rotation and axial shift. A 50 µm thick amorphous scintillator transformed the X-rays into visible light. The image was projected onto a CCD chip where the signal was digitized by means of an

analogue digital converter (ADC) and stored in computer hard-drive for further evaluation[1].
In this study, a CCD array detector with 1024 elements and 25 μm pitch was used.

Nominal isotropic resolution was set to 30 μm and integration time was set to 250 ms and 350 ms (G1 and G2). Image reconstruction was carried out by the implemented standard convolution back-projection algorithm.

## 4.3.2 Specimen preparation

In both G1 and G2 groups, 1-mm pure aluminum wire (99,999% purity, Alpha Aesar, Johnson Matthey GmbH, Karlsruhe, Germany) was longitudinally attached with adhesive to the side of each tooth as reference material. The apex of each root was cut to allow the tooth to be positioned into the center of a transparent polyacrylic cylindrical sample holder of 15.3 mm diameter. As no longitudinal experiment was conducted, it was not necessary to reposition the specimens in the sample holder. The long axis of G1 samples was positioned longitudinally in the sample holder, while that of G2 samples was positioned transversally. For the G1 group, this arrangement resulted in a complete circle of very dense tissue (enamel), which probably influenced the hardening of the beam in its path. On the other hand in the G2 group, enamel had only a small influence on X-ray attenuation (Figure 8).
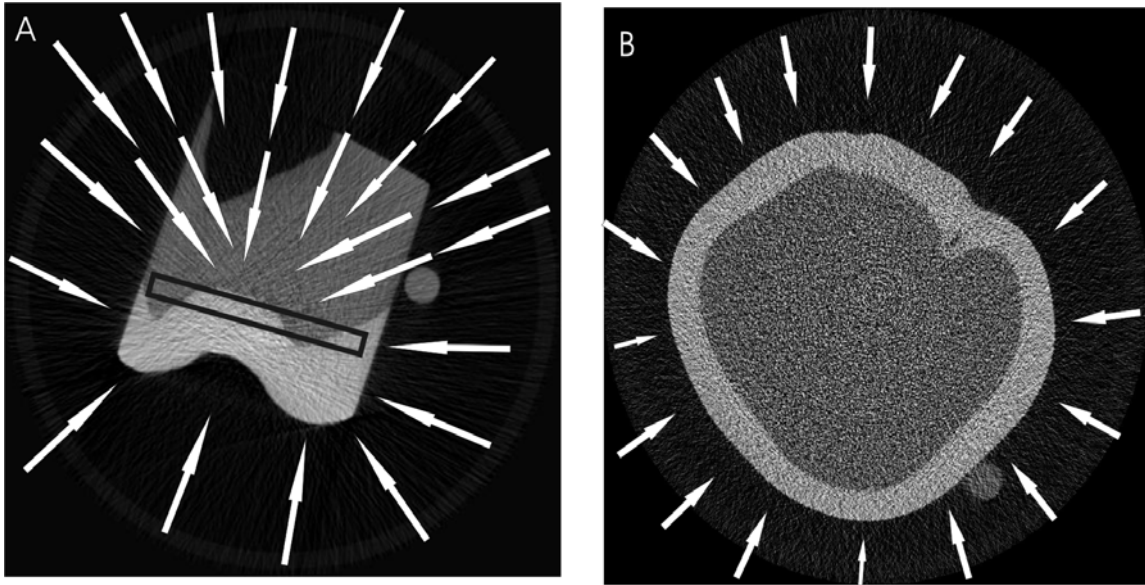
**Figure 8.** Image of a reconstructed slice showing the influence of dense areas on the results. "A" represents G2 and visualizes how beams easily reach enamel, even at its internal area (black rectangle). In "B" (G1) it is visualized that the beam has more difficulty to go through the whole sample due to a mantle of enamel, which is very dense and attenuates the X-ray more than dentin. The circle-shaped structure besides the tooth is a 1-mm pure aluminium wire.

To avoid drying artifacts, wet foam was positioned on top of the sample holder, which was sealed on the upper side with parafilm (Parafilm M, Pechiney Plastic Packaging, Chicago, USA), thereby maintaining a humid environment. The foam also mechanically fixed the specimen in the sample holder to prevent any small movement which is also a source of artifact in micro-CT images during the scan procedure.

### 4.3.3 Mineral concentration evaluation by micro-CT

Mean mineral concentration was measured using an image analysis software (ImageJ 1.32j, Wayne Rasband, National Institute of Health, Bethesda, USA), which is a public domain Java image processing computer program. Besides a large number of native functions, it enables two-dimensional measurements of mineral content through selected regions of interest. Each

image data set consisted of a stack of 15 micro-CT slices (1024 x 1024 pixels). At G1, 10 circular regions of interest (ROIs) (±64 pixels each) were drawn for each of the following tooth surfaces: external enamel, middle enamel, internal enamel (near amelodentinal junction, ADJ), external dentin (near ADJ), middle dentin, internal dentin (Figure 9). The ROIs were selected from the area between the end of the fissure region and the pulp chamber. Each selection excluded edges to preclude micro-CT partial volume effect (Dowker *et al.*, 2003).
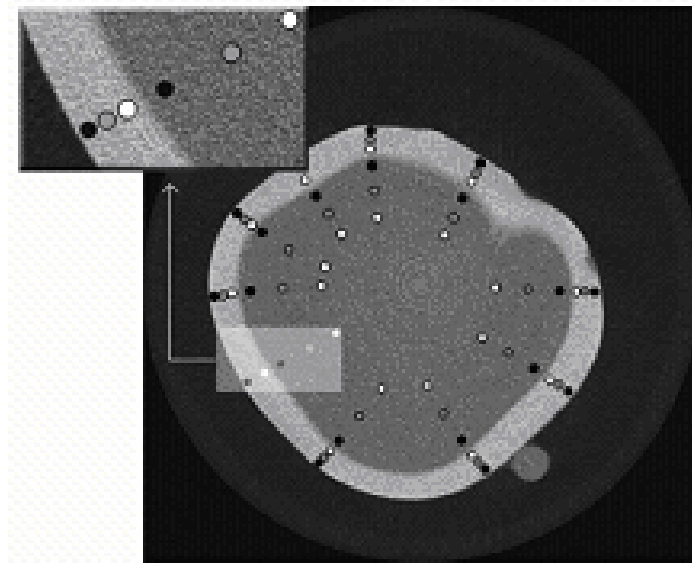


**Figure 9.** Two-dimensional micro-CT reconstruction image and selected ROIs in enamel and dentin. The rectangle in the upper-left side is a magnified image with detailed view of the ROIs. Black, grey and white dots are the external, middle and internal selection for each tooth tissue. The circle-shaped structure beside the tooth is a 1-mm pure aluminium wire.

At G2, the mean linear attenuation coefficient (LAC) for enamel and dentin were measured by histogram analysis after the application of two-means cluster algorithm (Isodata) for segmentation of tissues. To evaluate the gradient of MC through enamel and dentin surfaces, ROIs were also drawn.

Through first order calibration, LAC corrections were made based on published values for pure aluminum, which were obtained from the XCOM Photon Cross-Section database program (National Institute of Standards and Technology, Gaithersburg, USA) (Berger, 1999).

Assuming the mineral content in enamel to be pure hydroxyapatite with a density of 3.15 g/cm$^3$ (Angmar *et al.*, 1963), measured LAC for enamel (LAC$_e$) was converted to MC (C$_e$) (Wong *et al.*, 2004) by the following formula:

$$C_e = \frac{\mu_m \times \mu_{al\,(pub)}}{\mu_{al} \times \mu_{mhap}} \tag{4}$$

where $\mu_m$ is the LAC of mineral tissue, $\mu_{(pub)}$ the LAC of aluminum wire from published data, $\mu_{al}$ the measured LAC of the aluminum wire, and $\mu_{mhap}$ the mass LAC of hydroxyapatite (1.74 cm$^2$/g at 32 keV) from published data.

Since the images were previously calibrated and that published data and measured data for aluminum wire were the same, equation (4) can be simplified to:

$$C_e = \frac{\mu_m}{\mu_{mhap}} \tag{5}$$

## *4.3.4 Statistical analysis*

After the mean (± standard deviation, SD) MC value for every surface of the tooth was determined, one-way analysis of variance followed by Tukey's multiple comparison post hoc test were used to calculate the differences between the measuring sites. Overall significance level was set at P<0.05. Student's t-test was used to evaluate the significance of the MC differences in enamel and dentin between G1 and G2. All statistical tests were performed with SPSS version 12.0.1 (SPSS Inc. Headquarters, Chicago, Illinois, USA).

## 4.4. Results

Table 1 shows the mean MC values of enamel and dentin for G1 and G2. With the 6-mm dentin samples, the mean MCs of enamel showed a higher value as compared to the whole tooth sample.

**Table 1** Mean mineral concentration values and standard deviations for each group (G1 and G2)

| Group | Mineral Concentration (g/cm$^3$) | |
|---|---|---|
| | **Enamel** | **Dentin** |
| Mean G1 | 2.57 (± 0.12)[*] | 1.53 (± 0.12) NS |
| Mean G2 | 2.76 (± 0.03)[*] | 1.45 (± 0.02) NS |

Significant differences of the same tissue between G1 and G2 are indicated by '∗' corresponding to *P*<0.05.

In G1, the MC for enamel among all teeth varied between 2.43 (± 0.28) g/cm$^3$ and 2.75 (± 0.45) g/cm$^3$. To obtain the mineral content of the same area of interest from one slice to another, a z-profile was plotted. This z-profile contained additional information within the

thickness of each slice, which in the case of traditional microradiograms is integrated to only one value. Differences in mineral content in the same ROI from one slice to the next (30 μm in z-axis) showed a non-smooth mineralization pattern throughout the thickness (Figure 10). In G2, the mineral content ranged from 2.73 (± 0.30) g/cm$^3$ to 2.81 (± 0.35) g/cm$^3$. As opposed to G1, the variation in G2 from voxel to voxel of mineral content throughout the thickness did not show abrupt differences, whereby the differences were mostly around 0.05 g/cm$^3$ and rarely above 0.2 g/cm$^3$ (Figure 11).
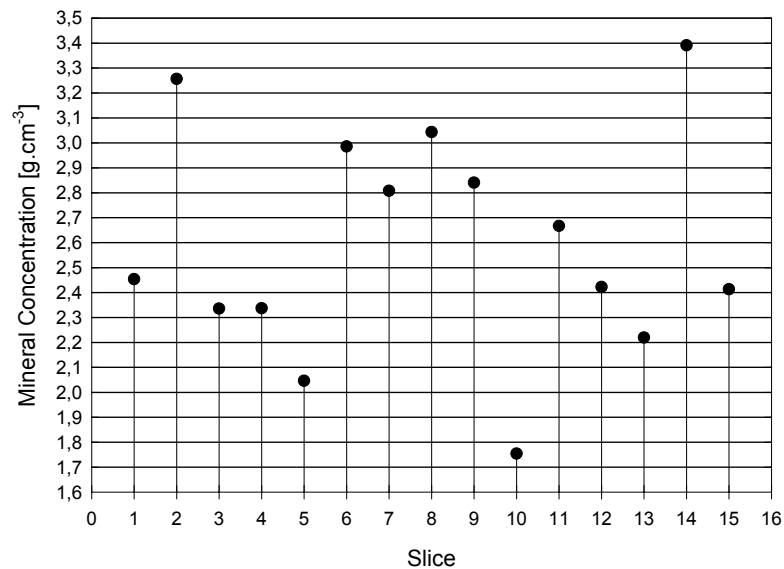


**Figure 10** Mean mineral concentration of ROI throughout the slices along the z-axis of G1, showing a high variation of the mineral concentration between the slices with a 30 μm linear resolution.
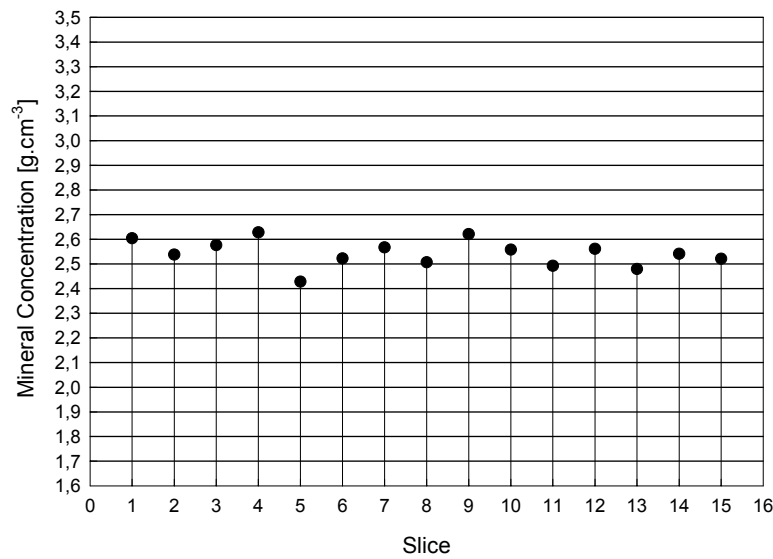
**Figure 11.** Mean mineral concentration of ROI throughout the slices along the z-axis of G2, showing little variation of the mineral concentration between the slices with a 30 μm linear resolution.

When analyzing the different enamel regions for both G1 and G2 (Table 2), the most external part and the middle part did not show any statistical significant differences. On the other hand, the internal part which was near to the amelodentinal junction (ADJ) had a lower MC with a statistically significant difference when compared to the other two enamel regions ($P<0.001$). The difference between external enamel and the enamel near ADJ was about 1.94% for G1 and 3.64% for G2. Student's t-test showed a statistically significant difference in overall MC among G1 and G2 for the enamel tissue ($P<0.001$).

**Table 2** Mean mineral concentration values and standard deviations in different tooth areas of enamel and dentin.

| Group | Mineral Concentration (g/cm$^3$) | | |
| --- | --- | --- | --- |
| | External | Middle | Internal |
| G1 enamel | 2.57 (± 0.29) | 2.58 (± 0.31) | 2.52 (± 0.33)* |
| G1 dentin | 1.51 (± 0.27) | 1.51 (± 0.22) | 1.45 (± 0.27)* |
| G2 enamel | 2.74 (± 0.11) | 2.73 (± 0.11) | 2.64 (± 0.14)* |
| G2 dentin | 1.49 (± 0.07) | 1.46 (± 0.06) | 1.36 (± 0.08)* |

Significant differences between areas of the same tissue and group are indicated by '∗' corresponding to $P<0.05$.

For dentin, results among teeth in G1 ranged from 1.36 (± 0.30) g/cm$^3$ to 1.69 (± 0.22) g/cm$^3$. For G2, the minimum MC value was 1.43 (± 0.23) g/cm$^3$ and the maximum was 1.49 (± 0.23) g/cm$^3$. Just like enamel, two distinct groups of dentin were defined: one consisted of the most external and middle dentin with no statistical differences, and the other consisted of the internal dentin with a decrease in mineral content toward the center of the tooth (Table 2). Difference between external and internal dentin was found to be about 3.97% for G1 and 8.72% for G2. When comparing the MC values of dentin between G1 and G2, there was a clear tendency towards a higher value for G1 although this difference was not significant ($P$=0.052). Throughout the z-axis, a similar pattern for the differences in mineralization degree was observed for dentin in both G1 and G2 as that described previously for enamel. In other words, a smoother difference was noted in G2 than in G1.

## 4.5 Discussion

In 1991, ten Bosch and Angmar-Månsson (ten Bosch and Angmar-Mansson, 1991) in a detailed review of quantitative methods to determine mineral changes recommended the use of radiographic methods to quantify mineral loss in whole teeth. The interest in radiation techniques is due to the ability of X-rays to travel through matter without destroying the specimens.

Currently, transverse microradiography (TMR) is considered as the 'gold standard' for the determination of mineral loss in experimentally induced incipient lesions. The method has been used for the comparison and validation of other newly developed caries diagnostic techniques (Damen *et al.*, 1997). A key disadvantage of microradiography lies in its superimposition effect, such that any non-uniformities detected in the direction of the X-ray beam are lost due to this effect. In addition, specimens need to be physically cut into thin sections which are rather difficult and definitely destructive. This is especially so for brittle materials or sections which include hard and soft regions such as caries lesions (Gao *et al.*, 1993). It has been reported that micro-CT requires no preparation of cut cross-sections (Bergmans *et al.*, 2001; Hahn *et al.*, 2004), and that it enables longitudinal experiments to be conducted in three-dimensional studies thereby overcoming the disadvantages of microradiography. The aim of this study was to test a commercial micro-CT device for the quantification of mineral content in tissues of a whole tooth or 6 mm-thick samples.

Our findings demonstrated that use of different methodologies led to different quantification values of mineral content. In G2, mineral concentration values of enamel were in agreement with past studies (Anderson *et al.*, 1996; Angmar *et al.*, 1963; Bergman and Lind, 1966;

Dowker *et al.*, 2003; Dowker *et al.*, 2004; Theuns *et al.*, 1986; Wilson and Beynon, 1989); in G1, statistically significant lower values were observed. The authors speculated that a few factors had caused the observed differences in results: a higher exposure time, the positioning of sample in the sample holder which can either facilitate or make it more difficult for the beam to pass through the sample, and in particular the reduction of sample size by eliminating the dense areas of enamel. Though we could not conclusively pinpoint which given factor influenced the results most, it was thought to be more related to the size of the sample as it highly affects the signal-to-noise ratio (Bonse and Busch, 1996; Wolfgang, 2001).

For the commercial device used in this study, it was recommended by the manufacturer to use samples up to 17 mm in diameter. However, these recommended instructions are usually more appropriate for bone studies. Recommendations for micro-CT analysis should be adjusted accordingly to the porosity or density of the specimen itself. In this study, the tooth specimen was an extreme compact mineral mass, thus attempt should be made to reduce the specimen size. This was done in line with the general rule of thumb where the energy of X-rays must be higher if the sample were thicker or denser (Bonse and Busch, 1996).

With regard to the analysis of different areas through the same tissue, neither Group G1 nor G2 yielded a consistent, smooth gradient from the external layer for both enamel and dentin in disagreement with that which was shown for enamel by Weatherell *et al.* (Weathere.Ja and Weidmann, 1967). Robinson *et al.* (Robinson *et al.*, 1971) showed that calcium and phosphorus concentrations were relatively high in the middle layers of enamel, which may explain the higher MC in this area for both groups in our experiment. A second possibility could be the incapability of the device to clearly define the gradient through tooth tissues. Nevertheless, lower values of mineralization were found in the innermost part of enamel, near to ADJ, which was consistent with past experiments (Angmar *et al.*, 1963; Dowker *et al.*,

2003; Wilson and Beynon, 1989). Many factors were associated with this gradient: variation in calcium and phosphorus contents, organic matter, water, and possibly variation in porosity.

When analyzing the MC values of enamel in G1, abrupt variation from one slice to the next (30 μm in z-axis) were seen throughout the thickness (Figure 10). These abrupt variations could be attributed to the high coefficient of variation and noise artifacts associated with the G1 settings. Hence, these abrupt changes were not observed in G2 (Figure 11) instead, the changes along the z-axis of 6-mm samples were smoother and rarely abrupt.

For dentin, the internal layer also appeared to have a lower degree of mineralization. The decrease in mineral content was already expected due to the following factors: greater amount and diameter of the dentinal tubules, as well as higher portion of water and organic phase. These factors clearly reduced the attenuation of X-rays from the ADJ to the internal layers of dentin. Similar results were already observed with micro-CT by Hayakawa *et al.* (Hayakawa *et al.*, 2000). However, these results disagreed with those of Anderson *et al.* (Anderson *et al.*, 1996), whereby a lower mineralization degree was indicated at the ADJ (1.42 g/cm$^3$) and a higher degree in deeper dentin (1.50 g/cm$^3$) using a non-commercial micro-CT device.

With the first-generation micro-CT system, practicable measurements of mineral content were limited to a small number of 'slices' through lesions formed in cut blocks with a 2x2.5 mm$^2$ cross-section (Dowker *et al.*, 2003). This need to physically cut specimens in order to measure mineral concentration ran contrary to one of the greatest advantages of the micro-CT system. In the present study which used a commercial, second-generation micro-CT device, it was once again shown that whole teeth are not recommended for quantification of mineral content. Thus, it is strongly recommended to consider the limited acceleration voltage of the μCT 20 system and to limit sample evaluation to 6-mm thickness which is already an advantage over

other analytic approaches which require the preparation of very thin, micrometric-sized samples. Concerning the accuracy of this device for longitudinal studies to quantify mineral changes, validation studies should be performed in order to provide the important supplementary information about the dynamics of treatment.

# Part II

# μCT vs. TMR:

# A Validation Study

# Chapter 5

# Measurement of Natural Caries Lesion by Quantitative Microradiography and Micro-Computed Tomography:

# A Correlation Study

## 5.1 Abstract

The aim of the current study was to investigate the correlation between micro-computed tomography and transverse microradiography. Therefore lesion depth and mineral loss of 13 natural enamel carious lesions were evaluated by both methods. In order to measure exactly the same slice in both methods, a special sample holder was prepared. For the TMR analysis start of lesion was defined as 20 vol%. However, for the micro-CT analysis four parameters were tested and compared for the start of the lesion; 0 vol% (G1), 20 vol% (G2), 25 vol% (G3) and 30 vol% (G4). After single factor analyses of variance (ANOVA), no significant statistical differences were found between the micro-CT groups; however, higher standard deviation was seen in G1. A strong Pearson correlation was found between micro-CT and TMR measurements. The following correlation coefficients were obtained for each group; mineral loss: 0.898, 0.928, 0.925, 0.917; lesion depth: 0.874, 0.854, 0.864, 0.879. It is

concluded that micro-CT can be used to measure mineral profiles through natural enamel carious lesions and a normalization of the start of the lesion at 20 vol% is meanfull for micro-CT evaluations.

## 5.2 Introduction

Over the past years there have been attempts to improve the development of techniques for caries detection and quantification. Ideally a method should be non-destructive in order to provide an insight into the dynamics of the procedure of interest, allowing longitudinal studies to be applied. Respective to the definition of caries as a non-static process, with disequilibrium of the de/remineralization balance, which leads to a mineral loss, the use of techniques that enable the tracking of mineral changes is desirable. The use of hardness measurements, polarizing light microscopy and conventional microradiography seems to be unsuitable for this purpose (Herkstroter *et al.*, 1990).

The direct relationship of radiographic methods to mineral loss and the feasibility to evaluate a large volume of data, including three-dimensional information, have increased the interest in micro-computed tomography (micro-CT). Further, because sectioning of samples seems to be a factor of variation and because of the increased demand of non-destructive methods, which enables measurements in whole tooth samples (ten Bosch and Angmar-Mansson, 1991), X-ray micro-computed tomography was considered for a future method of choice in validation studies (Huysmans and Longbottom, 2004).

The principle of micro-CT consists in reconstructing the linear attenuation coefficient, within an object, from measurements of the attenuation of an x-ray beam passing through the sample

at different viewing angles (Anderson *et al.*, 1996; Salome *et al.*, 1999). Each element of the projection is a line integral of the linear attenuation coefficient in the sample along the x-ray beam path (Salome *et al.*, 1999). A map of the linear attenuation coefficient can then be recovered from these line integrals using suitable reconstruction algorithms (Bonse and Busch, 1996; Kak and Slaney, 1988). Differences in linear attenuation coefficients among tissues are responsible for the X-ray image contrast.

Transverse microradiography (TMR) is, in these days, the most widely used method for validation of diagnostic methods (Huysmans and Longbottom, 2004). A few studies have been performed to evaluate enamel lesions by micro-CT and TMR (Dowker *et al.*, 2003; Dowker *et al.*, 2004; Gao *et al.*, 1993). Although these studies agree on the potential of micro-CT to give new insights into the demineralization process, according to Dowker et al. (2003), the mineral distribution observed from TMR line profiles will differ from those evaluated by micro-CT due to the differences of spatial resolution between both methods.

Considering both methods (Table 3), micro-CT works with higher energy, which allows scanning thicker samples, compared to TMR. Border artifacts and beam hardening, however represent some challenge in micro-CT analysis. As also recommended in TMR studies, a threshold at the beginning of the lesion could be necessary in order to meet a standard of the analysis, specially concerning to evaluations of lesion depth. Damen *et al.* (1997) have shown that a TMR image should be normalized by setting a threshold of 20 V% for the beginning of the lesion.

**Table 3.** Comparison between TMR and Micro-CT

| TMR | Micro-CT |
|---|---|
| Destructive - 80 µm thickness | *Non-destructive - whole tooth |
| Two-dimensional information | *Three-dimensional information |
| Short working-time | Long operational time |
| Single measurement | *Longitudinal measurements possible |
| Soft X-rays | Hard X-rays |
| Polychromatic - filtered | Polychromatic - filtered |
| No beam-hardening | Beam-hardening |

\* represents the advantages from micro-CT, which were sacrificed in this study

in order to compare both methods.

Regarding the lack of correlation studies between micro-CT and a traditional gold standard, the aim of this study was:

(1) to compare the integrated mineral loss and lesion depth from micro-CT and TMR of the same natural carious enamel specimen.

(2) to establish a threshold value to the beginning of the lesion.

## 5.3 Materials and Methods

### *5.3.1 Preparation procedure for enamel specimens*

Twenty enamel specimens selected for this comparative evaluation between TMR and micro-CT had been obtained from a pool of teeth stored in thymol 0.1%. These specimens provided areas of visually detectable white lesions, representing natural carious lesions. Thin plan-parallel sections of enamel were directly cut, perpendicular to the anatomical tooth surface,

with a diamond-coated saw with continuous water cooling (Mikroschleifsystem Exakt; PSI Grünewald, Laudenbach, Germany). Surfaces were polished with a hand tool (Figure 12) until a thickness of 70-90 μm was achieved and tested with a digital micrometer (IDU25, Mitutoyo Corporation, Japan). Before TMR analysis, images of the slices were obtained by histological light microscopy at X 5 magnification (Axioscop 2 MATin, Zeiss, Oberkochen, Germany) in order to assure the presence of carious lesions.
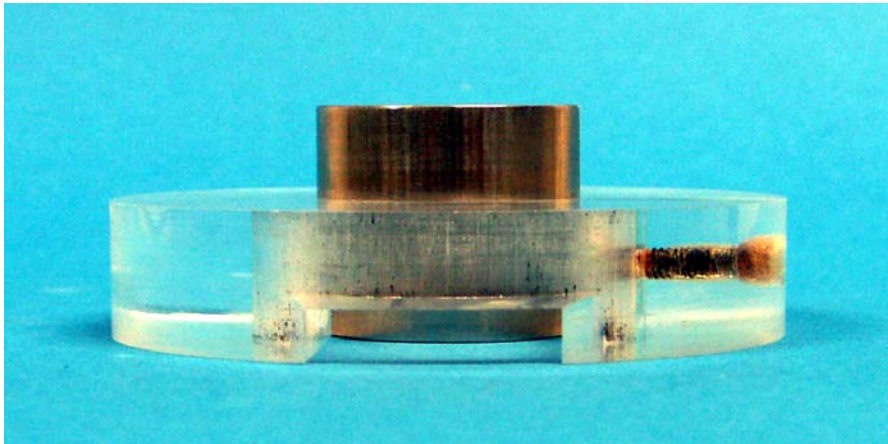


**Figure 12.** Hand tool for polishing the samples till the thickness of 70-90 μm.

## 5.3.2 Transverse Microradiography

Transverse microradiographs of the enamel specimens were obtained with a nickel-filtered copper (CuKa) X-ray source (PW 1830/40; Philips, Kassel, Germany) operating at 20 kV and 20 mA with a focus-specimen distance of 34 cm. From the tooth slice, together with an aluminum calibration step wedge, an x-ray projection of the microradiogram is made on high-resolution photographic film (high-speed holographic film, Kodak SO-253, Stuttgart, Germany). The exposure time was of 10 s. The film was developed under standardized conditions according to the manufacturer's recommendations.

The microradiographs of the sections were subjected to analysis using a digital image-analyzing system (CCD video camera Modul XC77E; Sony, Japan) that was interfaced to a universal microscope (Axioplan; Zeiss, Oberkochen, Germany) and a personal computer. Dedicated software (TMR 2000, Version 2.0.27.11; Inspektor Research Systems BV, Amsterdam, The Netherlands) was used to calculate the mineral content and depth profiles under the following defined parameters; start of lesion 20 vol%, start of sound enamel 95 vol% (end of lesion) (Arends *et al*. 1997) and 87 vol% mineral for the sound enamel (Angmar *et al.* 1963). TMR evaluation procedures are described in de Josselin de Jong *et al.*, (1987).

## *5.3.3 Preparation of sample holder for micro-CT measurements*

A great advantage of the micro-CT is its ability to measure whole teeth. In order to measure exactly the same slice in both methods, a special sample holder was prepared (Figure 13). After cutting the root of a sound molar tooth, another parallel cut was made at the upper third of the crown. A box of around the size of the enamel specimens prepared for the TMR measurements was made with a diamond bur in slow rotation on the inside-upper part of the tooth. This arrangement made it possible to include the slices into this tooth, for direct comparison of samples between the two methods. This was necessary in order not only to simulate a real situation, when the samples are non-destructively measured as a whole tooth, but also to respect the signal-to-noise ratio. I.e. the use of 70 kVp to scan this 70-90 μm samples would produce images without contrast resolution.
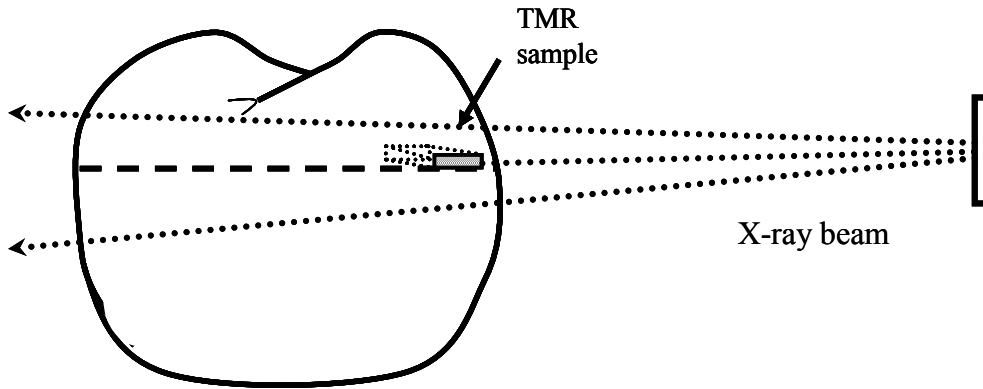
**Figure 13.** Schematic of the tooth used to position the samples to be scanned by micro-CT, which were prepared for TMR measurement  This procedure simulated a situation of whole tooth measurements by micro-CT and enabled comparison of exactly the same slice in both method (TMR x micro-CT).

## 5.3.4 Micro-Computed Tomography

Samples were scanned with a small-angle-cone-beam micro-CT (μCT 40; Scanco Medical AG, Bassersdorf, Switzerland) at 70 kVp and 114 μA, at a linear isotropic resolution of 8 μm. A 0.5mm aluminum filter was installed in the beam path to cut off the softest x-rays resulting in a detector response close to 31 keV. This was necessary to increase the accuracy of the beam-hardening correction, because in contrast to a synchrotron illumination, the use of polychromatic x-rays creates the problem of beam hardening.

The equipment used in this experiment offers some modalities of beam-hardening correction, through linearization technique by adding polynomial correction values to the measured projections. After pre-experiments, these correction values were best determined by scanning a homogeneous hydroxyapatite wedge of known density of 1200 mg HA cm$^{-3}$. The scanned wedge projection was compared to an ideal (monochromatic) projection (straight line for a wedge), and the difference between measured wedge projection and ideal projection was

fitted with a third order polynomial. This polynomial was used as the beam hardening correction function for subsequent tooth scans.

A hydroxyapatite phantom was also used to check the calibration of the system. Five different known densities were used (0, 100, 200, 400 and 800 mg/cm$^3$). Analyses of their attenuation coefficient and density values as well as their standard deviation were checked weekly to assure the stability of the X-ray tube.

For the scanning procedures each specimen was positioned into a transparent polyacrylic cylindrical sample holder of 16.4 mm diameter and mounted on a computer-controlled turntable, which synchronized rotation and axial shift. At an integration time of 3 s, 1000 projections were taken over 180°. Therefore 200 slices were selected, positioning the area of interest in the center of the stack (Figure 13). This procedure insured that the most perpendicular beams were achieving the sample. A 50 μm thick amorphous scintillator transformed the X-rays into visible-light. The image was projected onto a CCD-array-detector (2048 x 252 elements and 24 μm pitches) where the signal was digitized by means of an analogue digital converter (ADC) and stored to computer hard-drive for further evaluation. Reconstructions of the images were carried out by cone-beam algorithms in 2048 x 2048 pixels matrixes.

From the micro-CT stack, one slice of 8 μm z-axis resolution from each specimen was selected for the comparison purpose. The whole sample could not be evaluated by integration of all slices due to the tilting of the sample into the sample holder and consequent formation of artifacts, represented by shadows for one slice to the other in different areas of the images (Figure 14).
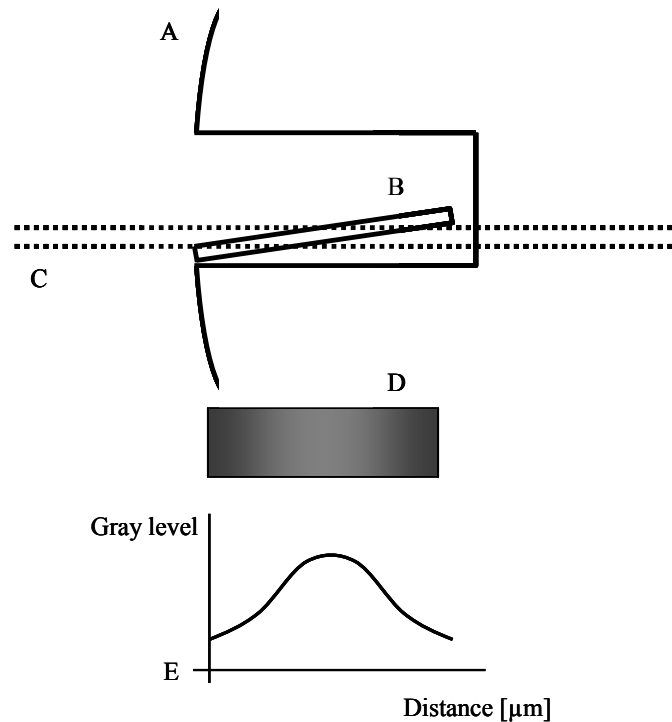
**Figure 14.** Representation of tilting of the sample and its consequence to the image. A. sample holder; B. sample; C. X-ray beams; D. image representation; E. graphic representation.

Regions of interest in enamel at comparable site to the TMR window were selected. Analyses of mineral loss and lesion depth were made using the same dedicated software used for the TMR analysis (TMR 2000, Version 2.0.27.11; Inspektor Research Systems BV, Amsterdam, The Netherlands). The choice for using the same software for both analyses was made in order to maintain the analysis of both methods as close related as possible and to be in a more controlled circumstance.

The complete TMR analysis is described in de Josselin de Jong *et al.*, (1987). Shortly, the TMR images are made by exposing both sample and aluminum step-wedge to an X-ray beam, in a photographic film. The calibration of those images are than made by fitting the corresponding optical transmission from the different aluminum gray-levels against the known aluminum foil thickness into a forth degree polynomial curve. Using the polynomial

function – p(T) – it is calculated the corresponding thickness aluminum thickness – $t_{Al, slice}$ (x) – for all values of optical film transmission and subsequently the thickness of the slice – $T_{slice}(x)$ – for the position x of the tooth slice.

$$t_{Al, slice}(x) = p[T_{slice}(x)] \text{ [m]} \qquad (5)$$

Later, the absorbance of the tooth slice – $A_{n, slice}(x)$ – at each position (x) can be calculated according to the equation:

$$A_{n, slice}(x) = \mu_{Al} \, t_{Al, slice}(x) \qquad (6)$$

Where $\mu_{Al}$ = 13.13 x $10^{+3}$ (m$^{-1}$) at monochromatic CuKα X-ray radiation (λ = 0.154 nm). (Int. Tables for X-ray crystallography, 1962).

The mineral volume percentage (V%) at position x is then calculated using the formula from Angmar *et al.* (1963):

$$V(x) = 100 \left( \frac{A_{n, slice}(x)/t - \mu_o}{\mu_m - \mu_o} \right) \text{ [vol \%]} \qquad (7)$$

Where t is the slice thickness; $\mu_m$ is the linear attenuation coefficient of mineral ($26.6 \times 10^{+3}$ m$^{-1}$, from crystallographic data of Young and Brown, 1983 and Int. Tables for X-ray crystallography, 1962), which is assumed to be pure hydroxyapatite [Ca$_{10}$(PO$_4$)$_6$(OH)$_2$]; $\mu_o$ is the linear attenuation coefficient of organic material with water inside the tooth ($1.13 \times 10^{+3}$ m$^{-1}$, from Angmar *et al.* 1963) at monochromatic CuKα X-ray radiation (λ = 0.154 nm).

As no step wedge calibration was used simultaneously within the micro-CT scans and this is mandatory for the evaluations in the software used in this study, it was necessary to simulate an aluminum step-wedge. Therefore, four grades of gray levels were conceded by the software manufacture and adapted for this analysis purpose. Also the resolution of the micro-CT could not be adjusted into the evaluation software. This resulted in relative values for our micro-CT analysis, which do not agree to the TMR evaluation values, but it is enough to answer the question of this study, if both equipments have or not any correlation, before further efforts are made in order to calibrate the system for this purpose.

The effect from border artifacts was tested by selecting four different parameters as thresholds points for the micro-CT evaluation (Figure 15):

**Group 1.** Start of lesion 0 vol%, start of sound enamel 95 vol% (end of lesion) and 87 vol% mineral for the sound enamel.

**Group 2.** Start of lesion 20 vol%, start of sound enamel 95 vol% (end of lesion) and 87 vol% mineral for the sound enamel.

**Group 3.** Start of lesion 25 vol%, start of sound enamel 95 vol% (end of lesion) and 87 vol% mineral for the sound enamel.

**Group 4.** Start of lesion 30 vol%, start of sound enamel 95 vol% (end of lesion) and 87 vol% mineral for the sound enamel.
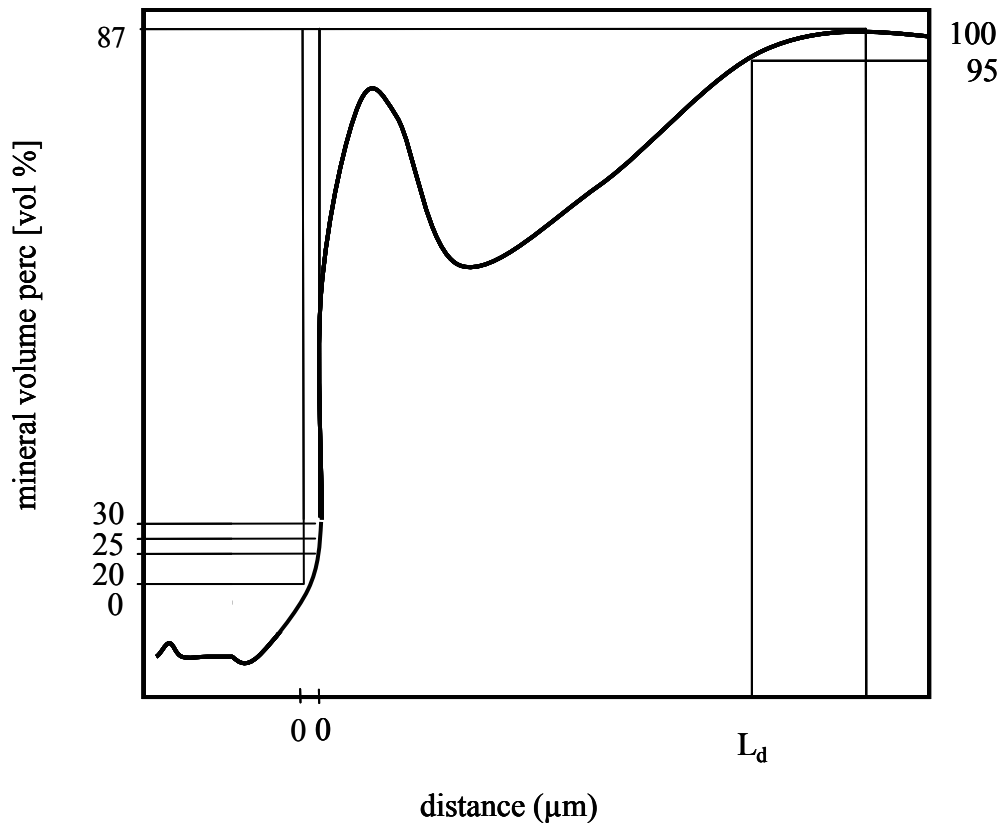
**Figure 15.** Variation in the definition of the lesion parameters. The start of the lesion (distance = 0) was defined by mineral contents of 0 vol%, 20 vol%, 25 vol%, 30 vol%. Lesion depth ($L_d$) was defined as 95% of the sound tissue. Figure modified from Damen et al. (Damen *et al.*, 1997).

## 5.3.5 Statistical Analysis

For each group, the mean, standard deviation and standard error were calculated for all measured parameter and analyzed using single factor analyses of variance (ANOVA) followed by post hoc Tukey's multiple comparison procedure ($\alpha = 0.05$). The correlations between TMR and micro-CT data (mineral loss (ML) and lesion depth (Ld)) were calculated using Pearson correlation coefficients. All statistical tests were performed with SPSS version 10.0.1 (SPSS Inc. Headquarters, Chicago, Illinois, USA).

## 5.4 Results

From twenty samples prepared for the TMR measurements, only 13 were used for the correlation purpose. The other seven samples were excluded due to the occurrence of artifacts. Figure 15 shows a typical formation of the scanning ring artifacts resulting from our micro-CT measurements. Although these ring artifacts can be present in micro-CT images, they were specially intensified in the areas of disconnected tissue, as in our arrangement with a slice into a free-spaced box. Another common artifact was due to a non-parallel positioning of the samples inside the tooth simulator, which disabled the evaluation. In these cases a shadow was created and no profile could be draw from these samples (Figure 16). It was then impossible to integrate all slices into one, what was the first proposal of the study, in order to compare the full TMR image with the full represented slices from the micro-CT images. For this reason, only one micro-CT slice (8 μm) was selected for each evaluation.

Profiles of mineral volume percentage from TMR and profile of relative mineral volume percentage from micro-CT were obtained at approximately equivalent positions through natural lesions. The one-way ANOVA for comparison of the micro-CT values between the threshold groups showed no statistically significant difference for mineral loss and neither for lesion depth. The descriptive statistics from these results are listed in tables 4 and 5. Figure 17 shows the profiles derived from TMR and micro-CT measurements plotted together. The higher peak observed at the subsurface lesions was always present in the micro-CT profiles, due either to the absence of micro-CT calibration into this analysis software or to the beam-hardening effect. Also a shorter length at the x-axis was due to an uncorrected scale of the micro-CT resolution into the TMR analysis software.
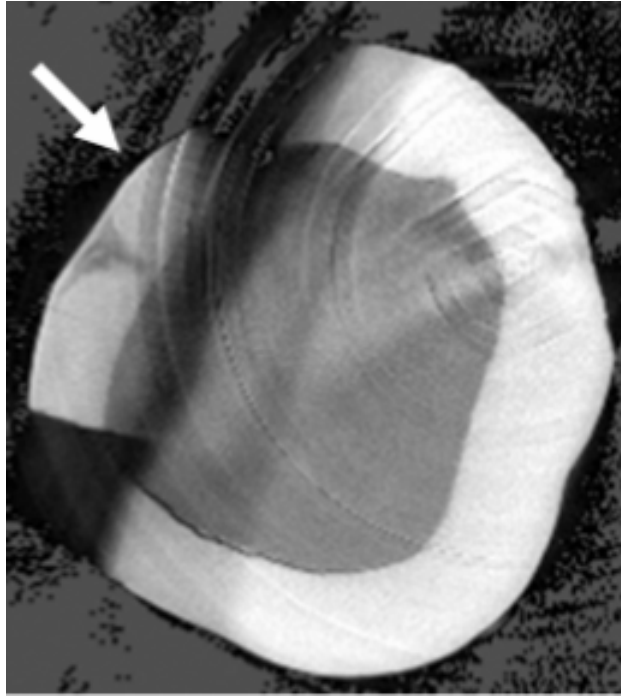
**Figure 16.** An image of the tooth scanned by micro-CT together with the TMR sample. The arrow shows the appearance of ring artifacts, especially when measuring thin slices, which was responsible for the elimination of some teeth for measurements of mineral loss and lesion depth.

**Table 4.** Mineral loss evaluation. Results are given in mineral "volume percentage per micrometer [v%.µm]".

|  | Mineral Loss | | | |
|---|---|---|---|---|
|  | Range | Mean | SE | SD |
| TMR | 2624.1 – 13883.6 | 6432.5 | 928.1 | 3346.3 |
| µCT group 1 | 1271.2 – 5231.1 | 2341.8 | 316.8 | 1142.3 |
| µCT group 2 | 961.7 – 4426.7 | 1945.0 | 285.0 | 1027.4 |
| µCT group 3 | 810.9 – 4251.8 | 1935.0 | 299.4 | 1079.4 |
| µCT group 4 | 825.2 – 4201.4 | 1972.0 | 296.9 | 1070.4 |

Group 1: normalization of surface at 0 V%; group 2: normalization of surface at 20 V%; group 3: normalization of surface at 25 V%; group 4: normalization of surface at 30 V%. Relative micro-CT values (non-calibrated).

**Table 5.** "Lesion Depth" evaluation. Results are given in micrometer [µm].

| | Lesion Depth | | | |
|---|---|---|---|---|
| | Range | Mean | SE | SD |
| TMR | 133.5 – 410.7 | 252.9 | 19.6 | 70.7 |
| µCT group 1 | 60.6 – 225.1 | 124.1 | 13.3 | 47.9 |
| µCT group 2 | 53.0 – 206.1 | 121.7 | 12.5 | 44.9 |
| µCT group 3 | 55.2 – 207.5 | 119.2 | 12.4 | 44.7 |
| µCT group 4 | 51.6 – 206.1 | 120.7 | 12.4 | 44.6 |

Group 1: normalization of surface at 0 V%; group 2: normalization of surface at 20 V%; group 3: normalization of surface at 25 V%; group 4: normalization of surface at 30 V%. Relative micro-CT values (non-scaled).
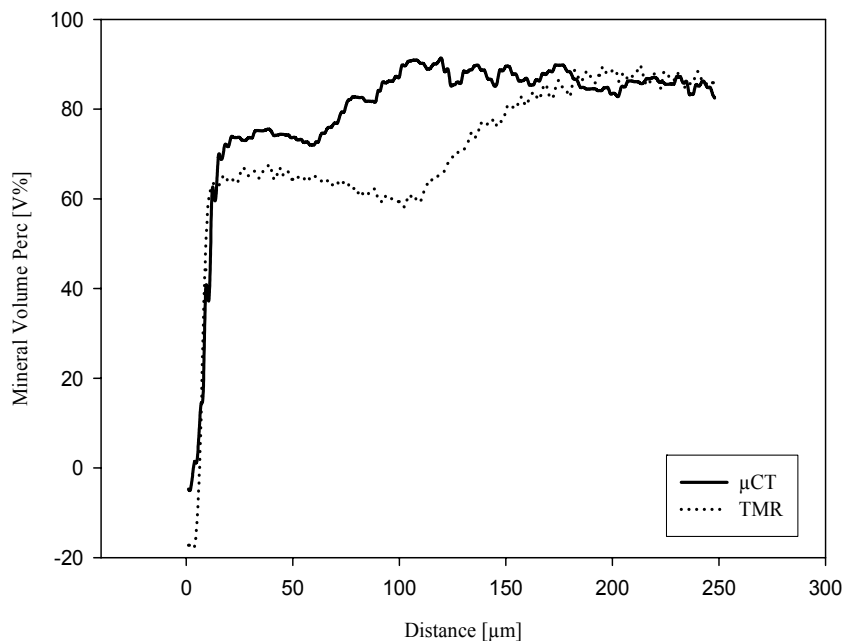


**Figure 17.** Profile line from TMR and micro-CT measurements through out a carious natural lesion in enamel. It can be observed that the traces are similar, but a highly attenuated subsurface lesion is present in the micro-CT profile. The difference in the extension of the lesion depth (x scale) can be explained by the evaluation software, which is set for the TMR resolution.

A strong Pearson correlation was found for the integrated mineral loss and lesion depth between TMR and micro-CT. The correlation coefficients for each micro-CT group and TMR are listed in table 5. The linear regression and confidence intervals (95%) for the mineral loss and lesion depth are given in figures 18 and 19.

**Table 5.** Pearson correlation coefficient between TMR and micro-CT evaluations of mineral loss and lesion depth.

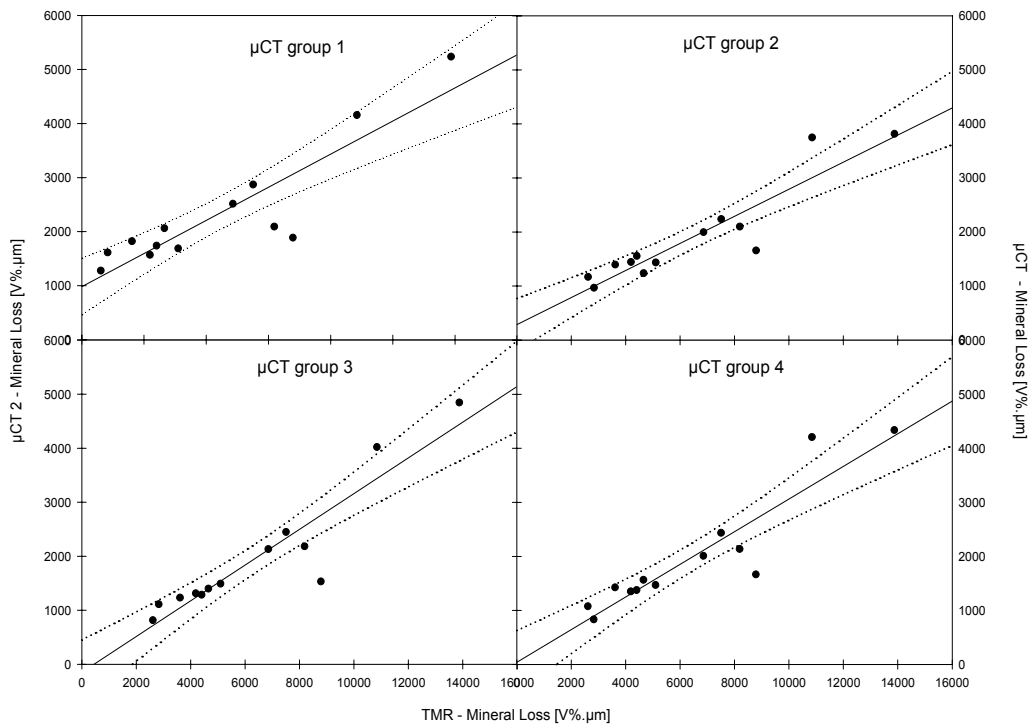| | Pearson Correlation | |
| --- | --- | --- |
| | Mineral Loss | Lesion Depth |
| TMR x µCT group 1 | 0.898 | 0.874 |
| TMR x µCT group 2 | 0.928 | 0.854 |
| TMR x µCT group 3 | 0.925 | 0.864 |
| TMR x µCT group 4 | 0.917 | 0.879 |



**Figure 18.** Comparison of mineral loss measured with TMR and micro-CT for each group. The continuous line is a linear regression and the dotted lines represent the confidence intervals (95%).

61

**Figure 19.** Comparison of lesion depth measured with TMR and micro-CT for each group. The continuous line is a linear regression and the dotted lines represent the confidence intervals (95%).
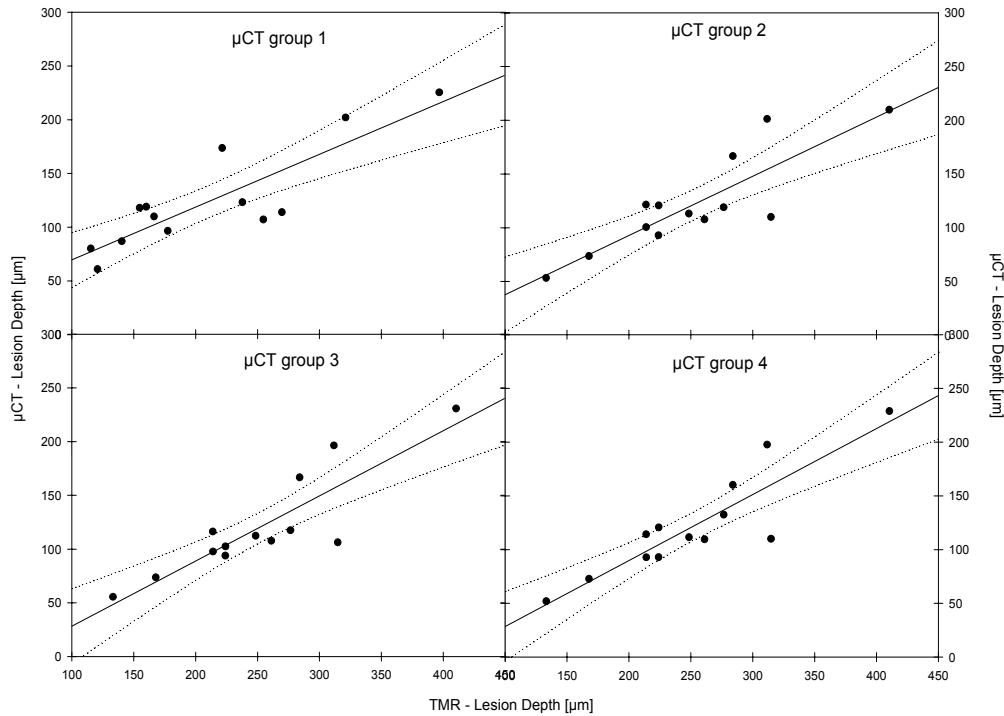
## 5.5 Discussion

The use of the microtomographic technique in dentistry is relatively new and still has the need to be evaluated and discussed, in order to find its limitations and gold purposes. A few universities have been giving effort, testing the technology, contributing to enhancement of physical properties, as resolution and reduction of artifacts, implementation of image analysis techniques to achieve common purposes as the higher quality, sensitivity and accuracy of the results.

One of the greatest collaboration of the micro-CT for dentistry research can be the evaluation of mineral content and the changes in dental hard tissue. However quantitative evaluations through micro-CT still wait for a well-established calibration method. As the results from scanning procedures are expressed in linear attenuation coefficient, the equivalence of this value to mineral content should be known.

The greatest problem related to the calibration of the measures is that the exact calculation of the effective energy resulting from the polychromatic measurements is very difficult to be achieved. As the linear attenuation coefficient is energy-dependent, the total attenuation, given by the logarithm of the ratio of the incoming and the attenuated X-ray beam, is no longer a linear function of the absorber thickness. The different X-ray beams of the polychromatic spectrum are not attenuated in the same way. Indeed, the lower X-ray energies will be easily absorbed, while the higher or harder energies are less attenuated. In other words, lower energy photons are removed preferentially from the X-ray beam as it passes through the object, resulting in a process called beam hardening. Therefore, the intensities in the projection images are not proportional to the object thickness, causing pronounced edges, streaks, and environmental artifacts in the reconstructed image, which may develop quantitative problems and complicates the calibration and density measurements. Therefore, the accuracy of the reconstructed CT values assumes that the attenuation of the incident X-ray beam is exponentially related to the thickness of the object, cfr. Beer's law. Furthermore, same materials can result in different grey values depending on the surrounding material, which is known as the environmental density artifact. Hence, the non-linear relationship between the attenuation and the material thickness makes the quantitative interpretation of the images more complicated (Brooks and Dichiro, 1976; Casteele, 2004; Young *et al.*, 1983).

For this reason this project was conducted under standardized conditions by using one single tooth as sample holder for simulation of non-destructive measurements. We could compare exactly the same slice evaluated by TMR in our micro-CT system. Further, because we are not testing the accuracy of our calibration in this study, our raw data were imported in the software analysis without any previous equivalence for mineral content and the values for micro-CT samples have only a relative meaning. Again, the choice for using the same software for both analyses was made in order to maintain the analysis of both methods as close related as possible and to be in a more controlled circumstance. I.e. the purpose of our study was to evaluate the correlation between micro-CT and TMR, as an important step for the validation of this system for caries research.

However we must point out that our study design was very disadvantageous for the micro-CT measurements. Ideally, tomographic imaging is usually performed on cylindrical samples in order to take advantage of the entire field of view and to avoid reconstruction artifacts at sample borders. Radiography on the other hand is best performed on parallel, polished plates in order to ease quantitative contrast analysis and to avoid spurious image contrast arising from surface irregularities (Wolfgang, 2001). The discontinuity between our tooth sample holder and the TMR specimen raised the formation of image artifacts. This means that in a real situation when no cuts would be performed, these image problems would be avoided.

It was also included in our set up the evaluation of different threshold to select the beginning of the sample, which is difficult due to the presence of border artifacts (Figure 20), common in micro-CT scans.
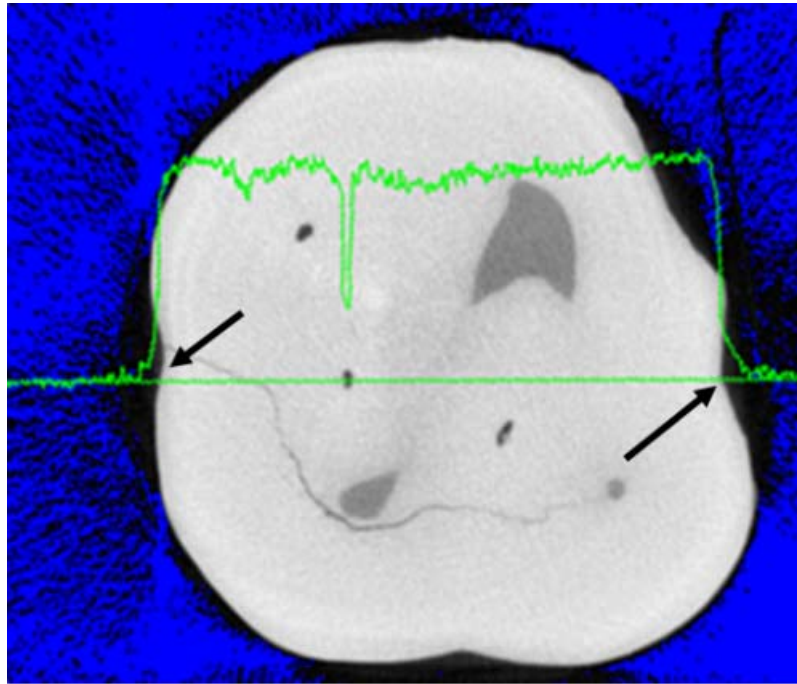
**Figure 20.** Image of a tooth by micro-CT and line profile showing the mineral content through out the sample. Arrows show the edge artifact at the surfaces of micro-CT images. It can be observed that the effect is higher in areas of irregularity of the sample.

In TMR evaluations it was already shown that non-perpendicular positioning of the samples to the surface leads to a shift in the lesion profile and that its contribution to the results after threshold of the mineral content of the surface layer at 20 vol% is negligible (Damen *et al.*, 1997). In our micro-CT images no statistical significant difference was found between the four micro-CT groups, which varied in their parameter for the start of the lesion (0 vol%, 20 vol%, 25 vol% or 30 vol%). Although group 1 had no statistical significant difference to the other groups, no standardization is possible due to a high variation of the effect of edge artifact in the beginning of the sample, which difficults the selection of the beginning of the sample, probably responsible for the higher standard error of the results. Therefore a threshold of 20 vol% also for micro-CT evaluations seems to be convenient. Further, an advice for future micro-CT experiment is to select the areas of interest, as the windows for de-remineralization experiments, where the surface is not or minimally curved.

A very strong Pearson correlation for mineral loss and lesion depth between TMR and micro-CT could be shown, with no difference between the groups. The option for mineral loss and depth of the lesion as parameters for the comparison was due to recommendations from the International Consensus Workshop on Caries Clinical Trial (Huysmans and Longbottom, 2004). According to Huyans and Longbotton, because of the higher variability of lesion depth and the definition itself of carious process, as a dynamic process, the mineral loss rate should have even a higher and preferred impact in validations studies. Random differences between both methods could be explained by the higher energy necessary to scan a whole tooth in micro-CT and consequently the polychromatic range of the X-ray beams. Enamel is an extreme dense tissue and the attenuation of the x-ray at the surface is too high. This could explain why the profiles showed higher peak at the subsurface lesion in comparison to TMR. The use of higher energy permitted us to scan whole tooth sample, but it could on the other side compromises the contrast resolution. Further research is necessary to test a calibration for the system and to establish the sensitivity of the equipment to detect very small artificial lesions or abrasion lesions in whole tooth samples.

In summary, although we offered a very disadvantageous situation for the micro-CT analysis it was shown that the method very well correlates with the TMR analysis for mineral loss and lesion depth evaluation of natural enamel carious lesions. Also we agree that threshold above 20 vol% as initial parameter is not necessary. The most valuable advantage of micro-CT is the measurement of whole tooth, permitting longitudinal experiments to be conducted and the possibility of three-dimensional non-destructive evaluations. Further efforts for the calibration and validation of the method for the future research in cariology are highly recommended.

# Part III

# Micro-CT and Dentin Study

# A Three-Dimensional Evaluation of Caries

# Chapter 6

# Micro-computed tomographic evaluation of a new enzyme solution for caries removal in deciduous teeth

## 6.1 Abstract

This study evaluated a new enzyme solution (SFC-V) for dentin caries removal compared with Carisolv™, both used with a prototype plastic instrument, this being a modified technique for Carisolv. Five deciduous carious teeth were sectioned and alternative treatments were applied to each half. Micro-CT observations showed that both treatments resulted in removal of the outer demineralized dentin layer with similar effects on deciduous carious dentin, removing 28.6% (SFC-V) and 28.2% (Carisolv) of demineralized tissue. Remaining demineralized dentin thicknesses of 0.27 μm (SFC-V) and 0.31 μm (Carisolv) were observed with no statistically significant difference. FE-SEM analysis demonstrated that the use of Carisolv resulted in a rougher surface whereas after enzymatic treatment, more organized dentin collagen, open tubules and only few bacteria were seen. In summary; the experimental enzymatic solution and the modified Carisolv treatment removed comparable amounts of carious dentin resulting in differing surface morphologies.

## 6.2 Introduction

Clinical dentistry in the twentieth century has been marked by a lack of complete understanding of the caries process, leading to a surgical approach and influenced by the properties of the restorative materials used, for example "extension for prevention" (Tyas *et al.*, 2000). After development of ultra-high speed rotary cutting instruments in the 1950s, cavity preparations tended to be larger. The limited lifetime of restorations lead to an era of "replacement dentistry", with additional weakening of the tooth structure after each therapeutic intervention and a constant round of failure of restorations (Hunter *et al.*, 1995).

In 1970, Kato and Fusayama (Kato and Fusayama, 1970a) reported the presence of two decalcified layers in carious dentin; a first soft layer, with very low calcium content and no capacity for remineralization, and a second decalcified layer with a mineral concentration somewhere between that of the first layer and normal sound dentin, which was considered to be remineralizable. Later, it was shown that collagens fibrils in the first layer are damaged at both the cross bands and the interbands, with minimal mineral content. This contrasts with the second layer which demonstrates clear collagen cross banding and interbanding with numerous apatite crystals in both the peritubular and intertubular dentin (Ohgushi and Fusayama, 1975).

The 70's also saw the first attempts at chemo-mechanical removal of caries when Goldman and Kronman (Kronman *et al.*, 1977) developed the GK-101 solution by adding Sorensen's buffer to sodium hypochlorite. After further work to replace glycine with amino butyric acid, the new version GK-101E, proved to be faster at softening demineralized carious dentin (Goldman and Kronman, 1976; Schutzbank *et al.*, 1978). However, the product, named

Caridex, was only available commercially up to the early 90's because of its slow procedure and the large volume of solution required (Beeley *et al.*, 2000).

Carisolv™ (Mediteam Dental AB, Sävedalen, Sweden) was introduced in 1988. The first version was formulated as a gel and was supplied in two syringes, requiring less volume per application and less time of operation than GK-101E. No special delivery equipment was required for its application; solution one, containing 0.5% sodium hypochlorite solution, was mixed with solution two, a pink viscous gel containing 15 mg of the amino acids lysine, leucine and glutamic acid, together with carboxymethylcellulose to make it viscous and erythrocin to make it readily visible (Beeley *et al.*, 2000). Recently, the gel has been reformulated to improve its efficciency. According to the manufacturer an increase in the amount of free chloramine was needed, which meant utilizing a higher concentration of NaOCl. The color agent has been removed and the new Carisolv gel is colorless. The pH of Carisolv reaches an approximate value of 12 prior to its use. After application of the solution treatment consists of excavation of caries tissue with specially designed steel hand instruments having sharp edges and blunt cutting angles.

One major drawback of the methods described so far is their lack of specificity and absence of self-limitation; the therapeutic endpoint is still assessed by visual and tactile methods. Color and hardness however are not good parameters on which to base a decision whether dentin removal should be continued or not during caries excavation (Hahn *et al.*, 2004). The presence or nor of bacteria after caries removal may be irrelevant if there is a good seal at the cavity margin as the caries progress is driven by a viable biofilm (Kidd, 2004). It would therefore be of great advantage to have a method that - in a gentle manner - specifically removes outer carious dentin and is self-limiting in the sense that remineralizable inner carious dentin is preserved. This should result in a maximum preservation of dentin.

Recently, an enzymatic approach to dentin caries removal has been proposed, which it is claimed fulfils these criteria. A prototype system has been developed (3M ESPE AG, Seefeld, Germany) comprising of a treatment solution (SFC-V) and a plastic hand instrument (STAR V1.3), which cannot remove dentin by itself. This solution essentially consists of a phosphoric acid/sodium biphosphate buffer of pepsin and a gelling agent. The hand instrument mechanically supports the treatment and is used to bring the solution into intimate contact with the dentin surface to be treated.

According to the manufacturer, the phosphoric acid dissolves the inorganic components of carious dentine, preserving healthy tooth structure, and gives the pepsin access to the organic parts of the carious biomass. The pepsin selectively dissolves denatured, but not native sound collagen. In order to avoid over excavation, the hardness of the hand instrument has been developed to have a hardness level between that of infected and sound dentin.

The aim of this study was to compare the effect of Carisolv and the new enzymatic method on natural carious extracted deciduous teeth. Although Carisolv treatment combines use of the solution with steel hand instruments, only the prototype plastic hand instrument was used. The evaluation was carried out using micro computed-tomography to measure the thickness of demineralized dentin retained after treatment and the volume of the removed dentin. FE-SEM images were taken to evaluate the quality of the retained dentin. The null hypothesis was that the new enzymatic procedure and Carisolv, when used in combination with the plastic instrument, would have a similar effect on dentin caries removal.

## 6.3 Materials and Methods

### 6.3.1 Sample preparation and treatment

Five deciduous carious teeth were selected for this study. One section (Leco VP100, LECO, Kirchheim, Germany) was made through the center of each caries lesion to obtain two groups, which were treated by either the new version of Carisolv (Carisolv™ Gel Multimix; MediTeam Dental AB, Gothenburg, Sweden) – Group A – or by SFC-V (3M ESPE AG, Seefeld, Germany) – Group B.

Both solutions were mixed according to the manufacturer's instructions. In order to test the effectiveness of the chemical or enzymatic treatment itself, it was decided to standardize the procedure by using a prototype plastic hand instrument (STAR V1.3, 3M ESPE, Seefeld, Germany) for both groups. In Group A, Carisolv was applied to the carious dentine and after 30 seconds the softened dentine was removed with the plastic hand instrument. The gel was applied several times until it no longer turned cloudy with debris. The cavity was then rinsed with water and gently dried. In Group B, the enzymatic solution was mixed and applied to the gently dried cavity until complete coverage of the dentin lesion was obtained. The plastic instrument was used to rub the cavity for 45 seconds. Additional SFC-V was added in cases of dense clouding. Subsequently, the cavity was rinsed with water, gently dried and visually examined. The procedure was repeated until no further clouding of the solution was seen.

The enamel side of each sample was longitudinally fixed to a plastic stick with fast glue, which itself was fixed in a base of polyether Permadyne Penta H (3M ESPE AG, Seefeld, Germany) to facilitate repositioning after treatment. Each block (sample/plastic-

stick/polyether) was then located in a cylindrical holder filled with distilled water to avoid dentin drying out of the dentin and to preserve the sample for further treatment. Both the outside of the sample holder and the polyether base were marked with an axial alignment line to allow positioning of the sample, and an alignment notch connecting the sample holder with the micro-CT turntable permitted a precise repositioning.

## *6.3.2. Micro-computed Tomography scans*

All samples were totally scanned before and after treatment with a small-angle-cone-beam micro-CT ($\mu$CT 40; Scanco Medical AG, Bassersdorf, Switzerland) at 70 kVp and 114 $\mu$A, at a linear isotropic resolution of 8 $\mu$m. A 0.5 mm aluminium filter was installed in the beam path to cut off the softest x-rays resulting in a detector response close to 31 keV. This was necessary to increase the accuracy of the beam-hardening correction, because in contrast to a synchrotron illumination, the use of polychromatic x-rays creates the problem of beam hardening. Beam hardening effects were also adjusted by adding polynomial correction values to the measured projections. These correction values were determined by scanning a homogeneous wedge of known density of 1200 mg HA cm$^{-3}$. The scanned wedge projection was compared to an ideal (monochromatic) projection (straight line for a wedge), and the difference between measured wedge projection and ideal projection was fitted with a third order polynom. This polynom was used as the beam hardening correction function for subsequent tooth scans.

The object was mounted on a computer-controlled turntable, which synchronized rotation and axial shift. At an integration time of 300 ms, 1000 projections were taken over 180°. A 50 $\mu$m thick amorphous scintillator transformed the X-rays into visible-light. The image was projected onto a CCD chip where the signal was digitized by means of an analogue digital

converter (ADC) and stored to computer hard-drive for further evaluation. A CCD-array-detector with 2048 x 252 elements and 24 µm pitch was used for this study. Reconstructions of the images were carried out by cone-beam algorithms in 2048 x 2048 pixels matrixes.

## 6.3.3 Data Evaluation.

### 6.3.3.1 Mineral concentration evaluation.

Assuming the mineral content of enamel to be pure hydroxyapatite with a density of 3.15 g/cm$^3$ (Angmar *et al.*, 1963), the measured linear attenuation coefficient for enamel ($\mu_m$) was converted to mineral concentration (C$_e$) (Wong *et al.*, 2004) by:

$$C_e = \frac{\mu_m}{\mu_{mhap}} \qquad\qquad (8)$$

Where $\mu_m$ is the linear attenuation coefficient of the mineral tissue, and $\mu_{mhap}$ the mass linear attenuation coefficient of hydroxyapatite (2.0352 g/cm$^2$ at 31 keV) from published data (Berger, 1999).

### 6.3.3.2 Volume analysis.

The three-dimensional evaluation of the image data involved the application of a constrained 3D Gaussian filter (width = 0.8, support = 1 or a kernel size of 3) to partially suppress the noise-artifacts in the volumes.

Line profiles were drawn in the two dimensional images to detect sound dentin. The attenuation values along this line were used as a guidance tool for the following selection of a visually assessed threshold, which was then arranged to 40.8 % of the maximum possible gray values. This represented a mineral concentration of 1.6 g/cm$^3$ or higher.

For calculation of the volumes before and after treatment a lower threshold was selected. I.e. not only the sound tissue would be included in the calculations, but also the carious or slightly demineralized tissues. Thus, all tissues which had 16.8% or higher of the maximum gray values were selected. This was the lowest acceptable value to be used, excluding interference from an edge effect between severaly demineralized tissue and water. This means that an equal or higher mineral concentration of 0.66 g/cm$^3$ was included in the calculations.

After evaluation of sound, pre-treated and after-treatment volumes, the percentage of caries tissue removed and demineralized dentin retained could be estimated relative to the whole of the demineralized tissue (Figure 21).
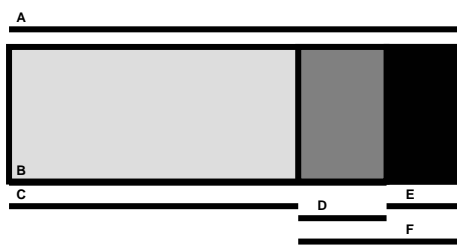


**Figure 21.** Schema for the volume calculation. A. Volume before treatment; B. Volume after treatment; C. Volume of sound tissue; D. Volume of slightly demineralized left dentin (B – C); E. Volume of removed caries (A – B); F. Volume of total demineralized tissue (D + E).

### *6.3.3.3 Thickness measurements.*

After treatment of the carious tissues, a demineralized area was still visible and measurable for both groups. The mean thickness of the demineralized area was assessed in a direct and three-dimensional way according to the method developed by Hildebrand and Rüegsegger (Hildebrand and Ruegsegger, 1997) for bone analysis. This estimates a volume-based local thickness by fitting maximal spheres to every point of the structure and further calculation of the volume-weighted mean thickness.
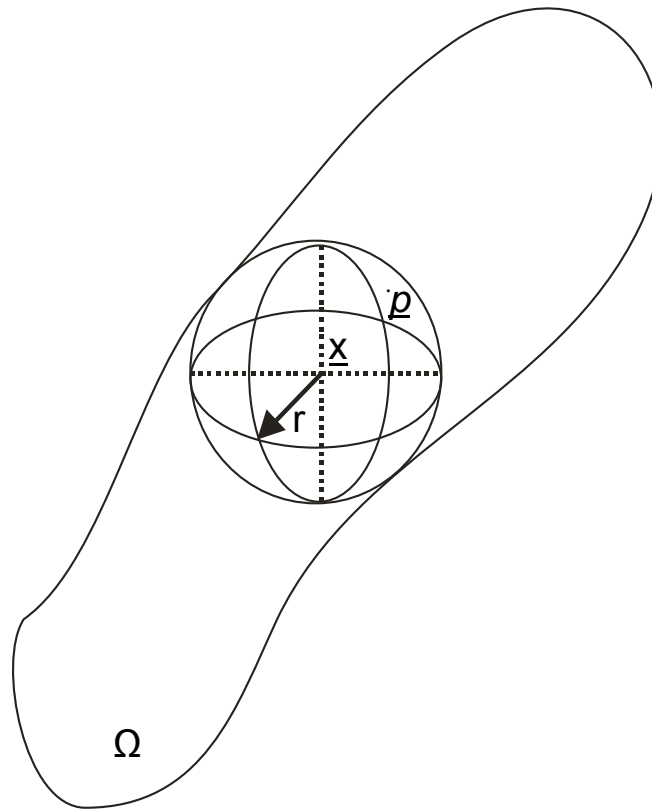


**Figure 22.** Figure modified from Hidelbrand and Rüegsegger [1997] for schematic demonstration of the local thickness $\tau(\underline{p})$ of a structure $\Omega$ determined by fitting maximal spheres to the structure.

Briefly, when $\Omega \subset R^3$ is the set of all points in the spatial structure under study and $\underline{p} \in \Omega$ is an arbitrary point in the structure, the local thickness $\tau(\underline{p})$ is defined by the largest sphere which contains the point $(\underline{p})$ and which is completely inside the structure (Figure 22):

$$\tau(\underline{p}) = 2 \cdot \max\left(\left\{r \mid \underline{p} \in sph(\underline{x}, r) \subseteq \Omega, \underline{x} \in \Omega\right\}\right)$$

(9)

Where $sph(\underline{x}, r)$ is the set of the points inside a sphere of centre $\underline{x}$ and radius r.

The mean thickness is defined by the arithmetic mean value of the local thickness taken over all points in the object:

$$\bar{r} = \frac{1}{Vol(\Omega)} \iiint_\Omega \tau(\underline{x}) d^3 \underline{x}, \qquad Vol(\Omega) = \iiint_\Omega d^3 \underline{x}.$$

(10)

Where d is the diameter of the sphere.

The maximum local thickness is equivalent to the diameter of the largest sphere that completes fits inside the structure:

$$\tau_{max} = \max\left(\left\{\tau(\underline{p}) \mid \underline{p} \in \Omega\right\}\right)$$

(11)

### 6.3.3.4 Calculation of Mineral Loss (ΔZ).

Using an image analysis computer program (ImageJ 1.32j; Wayne Rasband, National Institute of Health, Bethesda, USA), raw data from the micro-CT data set were imported and stored as 16-bit-signed integer values for further evaluation. From each sample three sets of 10 slices were selected for evaluation of the mineral loss. For subsequent analysis, the images were converted to 32-bit float and scaled by dividing the image by 4096 in order to achieve the linear attenuation coefficient, as recommended by the manufacturer of the micro-CT device. After conversion of values to mineral concentration as described above, the slices were averaged in the Z-projection to set an image of a single slice, similar to a transverse microradiographic (TMR) image of 80 μm. A rectangular area of interest was selected with a width of 20 pixels, from where a line profile could be calculated. The tracings of before and after treatment were used to calculate the $\Delta Z$, which is the integrated surface area (in g/cm$^3$ μm) above both profile lines (Gelhard and Arends, 1984; Mellberg *et al.*, 1985)

### 6.3.3.5 Calculation of the mineral concentration at the surface of treated samples ($I_{MC}$).

Evaluations of the outer, superficial mineralization status of the dentin left after treatment was estimated by selecting five regions of interest of 12 pixels (4 x 3) each in the slices prepared for mineral loss calculation. The result was the mean mineral concentration of the regions of interest in each sample.

## 6.3.4 FE-SEM Analysis.

After the caries removal and micro-CT procedures, the samples were sequentially dehydrated for 20 minutes in each of an ascending concentration of ethanol, from 50%, 75%, 87.5%,

93.75% to 100%. After the final ethanol procedure the specimens were dried by immersion in Hexamethyldisilizane (HMDS) for 10 minutes followed by air-drying at room temperature (Perdigao *et al.*, 1995). The specimens were then sputter-coated with a fine film of gold in a vacuum evaporator (Edwards S150B sputter coater, Edwards High Vacuum, Manor Royal, Crawley, England) at 7-8 mA for 1 minute. The prepared specimens were analyzed with a field-emission scanning electron microscope (LEO 982, LEO Electron Microscopy, Inc One Zeiss Drive, Thornwood, NY 10594) at 10kV and a working distance of 16mm at magnifications of 1000x, 5000x and 10000x.

### *6.3.5 Statistical Analysis.*

After the mean values for the volumes, thickness, $\Delta Z$ and $I_{MC}$ for every sample had been determined; the Student *T*-test was used to calculate the overall significance level at $P < 0.05$ for the differences between treatments. All statistical tests were performed with SPSS version 12.0.1 (SPSS Inc. Headquarters, Chicago, Illinois, USA).

## 6.4 Results

Prior to carrying out the three dimensional evaluation, the images were analysed two dimensionally. A line profile was used as guidance for the establishment of a threshold for sound tissue. This permitted the observation of sound dentin and the two different regions of demineralization; An area of highly demineralized dentin, and dentin with an increasing area of mineralization (Figure 23). The average mineral concentration at the transition zone between these two demineralized layers was 0.59 ($\pm$ 0.05) g/cm$^3$. Both treatments removed demineralized tissue beyond than this transition area (see below).
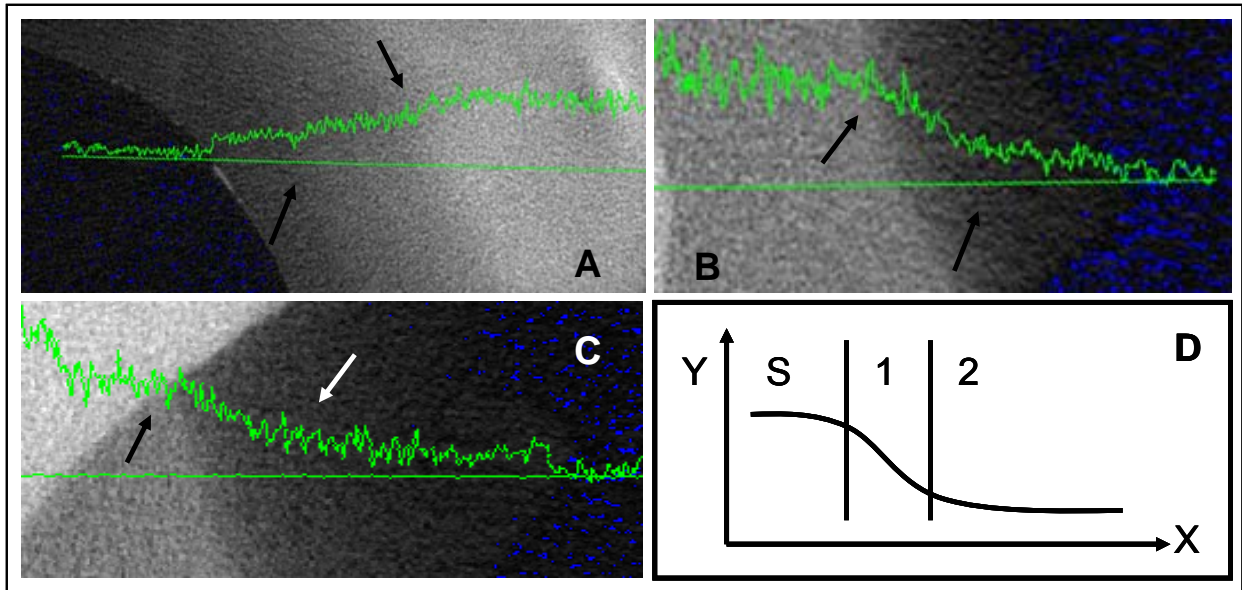
**Figure 23.** Two-dimensional micro-computed tomographic images of demineralized carious dentin showing the presence of two layers. A, B and C, represent the highly demineralized layer; an intermediate layer with increasing degree of mineralization and a sound dentin layer, respectively (limits represented by arrays). D shows a representative profile of the different layers of carious dentin. S, sound dentin; 1 inner carious layer; 2 outer carious layer; coordinate Y, mineral concentration; coordinate X, distance.
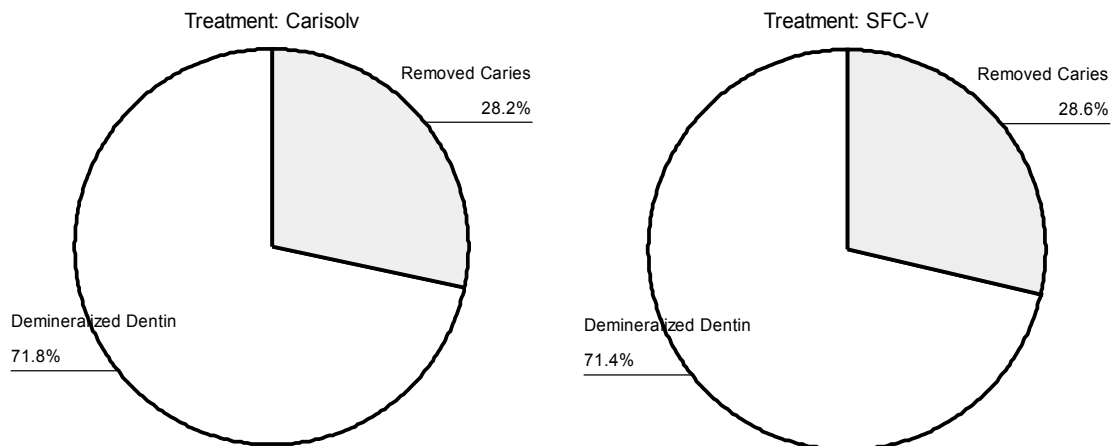


**Figure 24.** Diagram of the distribution of removed dentin and retained demineralized dentin after caries treatment with chemical and enzymatic solutions, showing a similar pattern of caries removal for both treatments. In white, the left demineralized dentin and in traces the removed carious tissue.

The volume-based local thickness of the demineralized layer left by both caries removal treatments is given in Table 6. Again, no statistically significant difference was found between the treatments. These data show the similarity between the chemical and enzymatic procedures for caries removal in deciduous teeth. Figure 25 shows a three dimensional evaluation of the volume-based local thickness.
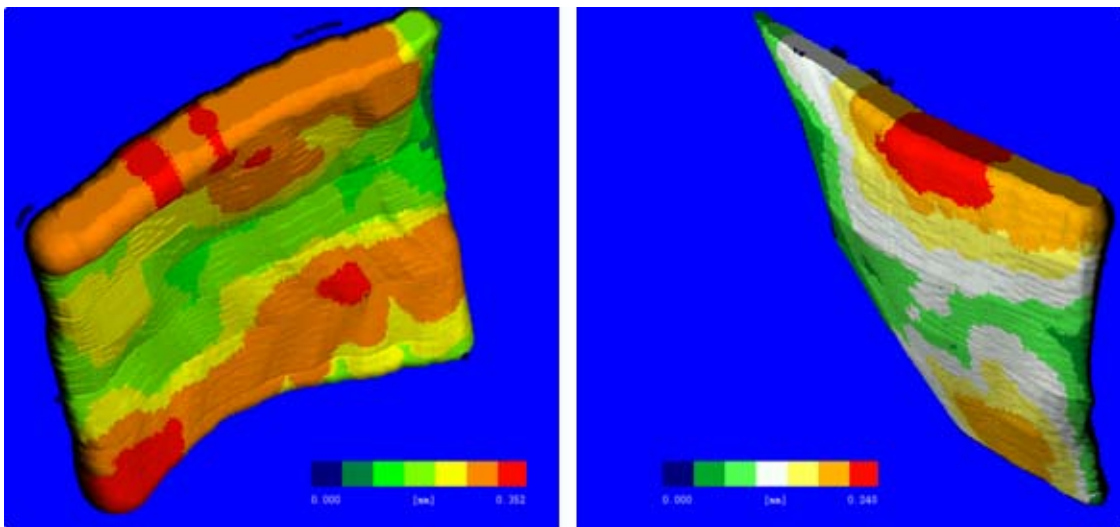


**Figure 25.** Typical image of the retained demineralized dentin. Colors represent different degree of thickness in mm. The volume tended to have a smooth regular form, with more volume of demineralized dentin at the borders. A – Carisolv sample; B – SFC-V sample.

Traditional profile tracings were drawn in the simulated microradiograms for calculation of $\Delta Z$. The mineral loss calculated for the line profiles prior to any treatment presented no statistically significant difference between groups, indicating that any alteration to the statistical outcome after treatment is a treatment effect. The values of mineral loss after treatment are shown in Table 7, and again no statistically significant difference was found between treatments (p = 0.8).

**Table 6.** Volume-based local thickness of the demineralized dentin layer.

| Sample | Carisolv | SFC-V |
|---|---|---|
| | Mean (SD) | Mean (SD) |
| 1 | 0.26 (± 0.09) | 0.28 (± 0.07) |
| 2 | 0.25 (± 0.05) | 0.26 (± 0.06) |
| 3 | 0.20 (± 0.07) | 0.14 (± 0.04) |
| 4 | 0.65 (± 0.24) | 0.45 (± 0.12) |
| 5 | 0.21 (± 0.06) | 0.22 (± 0.06) |
| **Mean** | 0.31 (± 0.18) | 0.27 (± 0.11) |
| **SE** | 0.08 | 0.05 |

No statistically significant difference was found between groups ($p = 0.68$).

**Table 7.** Mineral loss analysis after treatment of caries ($g/cm^3$ μm).

| Sample | $\Delta Z$ Carisolv | $\Delta Z$ SFC-V |
|---|---|---|
| 1 | 294.46 | 375.69 |
| 2 | 503.49 | 546.52 |
| 3 | 254.76 | 289.16 |
| 4 | 472.45 | 426.33 |
| 5 | 176.76 | 180.65 |
| **Mean** | 340.38 | 363.67 |
| **SE** | 63.35 | 61.87 |

Analysis by Student T-test gave no statistically significant difference between treatments ($P = 0.8$).

The mean mineral concentration in g/cm$^3$ was also measured within regions of interest in the superficial tissue left by both treatments. Although the SFC-V group (0.90 ± 0.16) tended to leave a slightly higher amount of mineralized dentin compared to Carisolv (0.85 ± 0.13), no statistically significant difference was observed between the groups (p = 0.05).

The FE-SEM analysis evidenced different morphological appearance between the two groups (Figure 26). Group B showed a low number of opened tubules, high numbers of bacteria and no clear collagen phase in the treated dentin, whereas in Group A, the prevalence of open tubules, few signs of bacteria, and a highly structured inter-tubular collagen network could be observed.
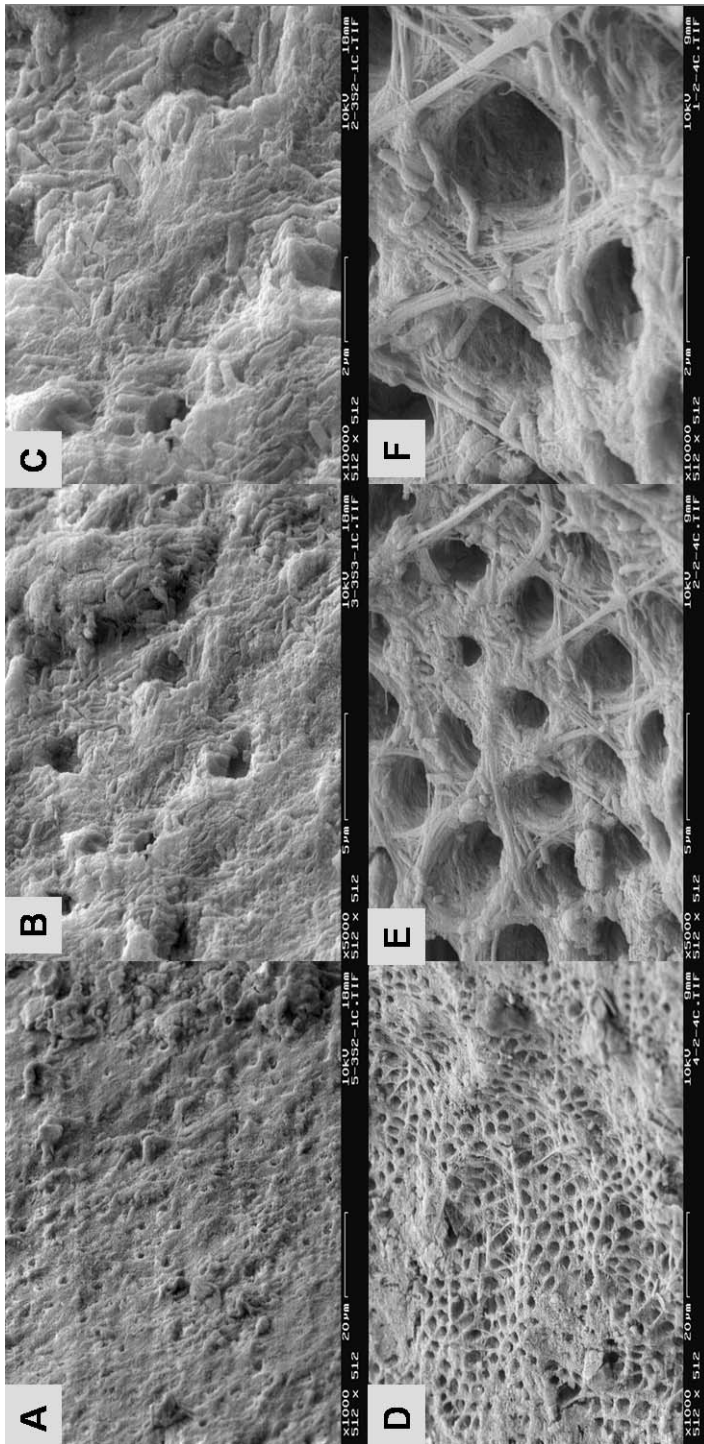
**Figure 26.** FE-SEM images of the dentin surfaces after chemomechanical and enzymatic treatment. A, B and C show x1000, x5000 and x10000 views of the dentin surface after treatment with Carisolv, showing evidence of a rough surface, with some smear layer and many bacteria. D, E, F show x1000, x5000 and x10000 images of dentin after treatment with SFC-V showing a greater frequency of open tubules, little evidence of smear layer, more organized collagen fibres and few bacteria.

## 6.5 Discussion

The chemomechanical caries removal technique gained interest in dental researches due to its concept of tissue preservation while insuring removal of the denatured collagen-phase dentin. Although Sato and Fusayama (Sato and Fusayama, 1976) have shown that the two layers of infected and affected dentin can be delineated by fuchsin staining, it is still a very subjective and technique sensitive method. The use of dye as a factor in over preparation of a cavity at the amelo-dentinal junction and pulpal surface has been clearly demonstrated (Kidd *et al.*, 1993; Yip *et al.*, 1994). In addition, in this era of esthetic and adhesive dentistry any remnant of color stain is not acceptable. Thus, a self-limiting caries removal therapy is the best alternative to preserve remineralizable tissue and to prevent over excavation of the cavity.

The action of Carisolv on carious dentin is still not completely understood. Habib et al. (Habib *et al.*, 1975) reported disruption of degraded collagen in carious dentin by chlorination of hydroxiproline in the collagen molecule. Hydroxiproline is converted to pyrrole-2-carboxylic acid and the quartenary superhelix is destroyed. Tonami et al. (Tonami *et al.*, 2003) have shown that the amino acids present in Carisolv may be responsible for the reduction in aggressiveness of sodium hypocloride on sound dentin and the inner layer of carious dentin.

The new enzymatic solution for caries removal is based on pepsin. The use of limited pepsin digestion for solubilization of collagen is well known (Kuboki, 1991; Miller and Rhodes, 1982). Pepsin splits collagen polymers into monomers, acting specifically on non-helical collagen, which contains inter- and intra-molecular cross-linking (Tonami and Ericson, 2005). Flückiger et al. (Fluckiger *et al.*, 2005) conducted a histological study on the remaining carious dentin left by Carisolv but considered that a three-dimensional evaluation was needed

for a better understanding of its action. In this perspective, micro-computed tomography (micro-CT) potentially represents a key tool, especially in caries research, since it allows high spatial resolution records of inner structures (Rossi *et al.*, 2004), three-dimensionally and without destruction of samples (Lin and Miller, 1996).

According to our images, micro-computed tomography was sensitive enough to detect the two layers of carious dentin, in accordance with work by Kato and Fusayama (Kato and Fusayama, 1970b) using optical microscopy and electron microprobe analysis. Our results also demonstrated the very low mineral content present in the outer, superficial layer ($< 0.59$ g/cm$^3$), and a gradient of increasing mineral content in the direction of the sound dentin. As the initial mineral concentration found by both groups A and B was 0.85 and 0.90 g/cm$^3$, we can assume the ability of both treatments to remove the first very demineralized layer of carious tissues even without the use of steel instruments.

Similar volumes of carious tissue were removed by Carisolv and SFC-V. The volume-based local thickness of the demineralized layer left after treatment showed no statistically significant differences between the groups; however we found a much higher value for the thickness of the demineralized residual layer in our study compared with the literature. When Kato and Fusayama (Kato and Fusayama, 1970a) first reported the presence of the two layers in carious dentin, they described a very thin second layer of only 50-80 µm. These teeth had been demineralized artificially using a decalcifying solution for ten minutes (Kato and Fusayama, 1970a), which was expected to yield smaller lesions compared to natural carious teeth. Our results are also not in agreement with other studies which have used naturally carious teeth for chemomechanical treatment. After application of N-monochloro-DL-2-aminobutyric acid (NMAB) or NMAB containing 2 mol/l urea, Yip et al. (Yip *et al.*, 1995) occasionally found areas of 0.05 to 0.1 mm of remaining demineralized dentin, and Flückiger

et al. (Fluckiger *et al.*, 2005) found 0.18 mm and 0.16 mm residual dentin caries thickness for Carisolv and hand excavators. In the present study it was expected that higher values (0.32 mm and 0.27 mm for Carisolv and SFC-V) would be obtained because we opted for not using a sharp metal instrument for excavation of the softened tissue, but a plastic instrument, as recommended for use with SFC-V.

One major drawback of the use of sharp instruments is their lack of specificity and absence of self-limitation. It would therefore be of great advantage to have a method that results in a maximum preservation of dentin. Akimoto et al. (Akimoto *et al.*, 2001) demonstrated in-vivo an increase in nano-hardness and measured calcium levels at non-resin impregnated demineralized dentin layers, which became remineralized after a period of 6-months following the adhesive resin treatment. Remineralization of carious dentin has also been evidenced by enhanced hardness and reduction in bacterial growth after stepwise excavation of deep dentin caries (Bjorndal *et al.*, 1997; Bjorndal and Thylstrup, 1998; Bjorndal and Larsen, 2000).

Although not statistically significantly different, the enzymatic solution tended to remove a greater amount of caries compared to Carisolv. From the FE-SEM images there appeared to be a difference in the effect the two groups had on carious dentin. In Group A, a rough, non-organized infected layer of dentin was observed, while in Group B, dentin was more organized, patent dentin tubules were present and few bacteria were seen. This may be explained by the different mode of action of the two solutions. As claimed by the manufacturer, the acid in the enzyme solution may have dissolved remnant hydroxyapatite during treatment and consequently no smear layer was generated. This effect would not be seen at the basic pH (12) of the Carisolv solution, therefore, it is necessary to maintain the mechanical excavation procedure for Group A, using the recommended metal hand

instrument with Carisolv solution [cf. (Azrak *et al.*, 2004; Lager *et al.*, 2003)]. This procedure may, however, result in a non-self-limiting procedure and lead to over-excavation of dentin from use of the sharp instruments. As stated earlier, it is considered that it would be a major advantage to have a caries removal method that gently and specifically removes outer carious dentin, and is self-limiting in the sense that remineralizable inner carious dentin is preserved.

Studies of dentin caries have shown a specific link between the destruction of the collagenous matrix and the loss of firmly bound mineral (Frank *et al.*, 1964; Johansen and Parks, 1961; Selvig, 1968). A systematic evaluation of this retained collagenous phase is needed to establish whether it is still intact (Kuboki *et al.*, 1977) and/or contains enough mineral for the promotion of remineralization (Daculsi *et al.*, 1979; Levine and Rowles, 1973; Tveit and Selvig, 1981), before we can exclude the use of these sharp instruments, as in this study. On the other hand, Klont and ten Cate (Klont and ten Cate, 1990) have shown that removal of exposed collagen did not affect the rate of mineral deposition and that remineralization of dentin occurs by precipitation onto residual hydroxyapatite crystals. It could be therefore, that the residual dentin, although less well mineralized than sound dentin, offers a source of deposition and/or growth of new mineral, leading to arrest or reversal of caries at these locations.

## 6.6 Conclusion

In summary, Carisolv and the experimental enzymatic solution removed comparable amounts of deciduous carious dentin, when used in combination with a prototype plastic instrument. A layer of partially demineralized dentin was retained after the completion of the caries removal treatment, this layer being thicker than has previously been reported, indicating that more

tissue had been preserved. Additional research is necessary to evaluate the quality of the remaining collagen and the possibility of crystal growth and mineral apposition at this demineralized layer. The use of Carisolv with the plastic hand instrument did not appear to remove all the infected carious dentin. The manufacturer's recommendation to use Carisolv with metal hand instruments seems to be valid; however this may lead to a non-self-limiting procedure resulting in over excavation of the cavity from use of sharp instruments.

# Summary

Over the past years there have been attempts to improve the development of techniques for caries detection and quantification. The demand for a non-destructive method has encouraged the use of micro-CT in studies of enamel de-remineralization. Our contribution to this development were presented in this work by evaluating the limitations of the method concerning energy and the size of the samples, by correlating the micro-CT results of mineral loss and lesion depth with a gold standard (TMR), and by suggesting a three-dimensional model for the study of dentin caries excavation methods.

After a literature review, which is the content of the first and second chapter of this work, we evaluated a second generation fan-beam commercial micro-CT ($\mu$CT 20, SCANCO Medical AG, Bassersdorf, Switzerland) for mineral content quantification. According to our results, the machine that works at 50 kVp and 160 $\mu$A is not feasible to quantify the mineral content of whole tooth. Thus, we strongly recommended to consider the limited acceleration voltage of the $\mu$CT 20 system and to limit sample evaluation to 6-mm thickness which is already an advantage over other analytic approaches which require the preparation of very thin, micrometric-sized samples.

The correlation of micro-CT and TMR was evaluated in our second experiment, written in chapter 5. After exposing 70-90 $\mu$m slices with natural carious lesion in enamel by a TMR equipment, micro-CT measurements ($\mu$CT 40; Scanco Medical AG, Bassersdorf, Switzerland) were made inserting these samples inside a whole tooth which was especially prepared in order to simulate a non-destructive evaluation. Also the effect of edge artefact was evaluated by using different threshold for the start of the lesion. Our observation showed the high

Pearson correlation between both methods for evaluation of mineral loss and lesion depth and that the variation of the lesion parameter as 20 v% for the beginning of the lesion is a rational procedure. Above this value seems to be not necessary and 0 v% can lead to a higher variation of the values due to operator uncertainties within an artefact area.

With respect to the use of micro-CT in dentin excavation research, it was a valuable tool to distinguish between the three mineralization phase in the carious process; a very high demineralised dentin, a layer of increasing mineralization and a sound dentin layer. In this chapter we have compared a new enzyme solution (SFC-V, 3M ESPE AG, Seefeld, Germany) for dentin caries treatment in comparison with a well established method (Carisolv™ Gel Multimix; MediTeam Dental AB, Gothenburg, Sweden). The use of the threshold technique for the evaluation of the removed and remaining dentin after excavation seems to be worthwhile. The mathematical model could very well compare both solution and the remaining thickness of demineralised dentin with additional insight into its three-dimensional perspective.

In this work we tried to demonstrate the current possibilities of micro-CT imaging and quantification for the use in caries research. The system presents its limitation with respect to energy selection, scans artefacts, calibration and costs. However, our caries research domain demands a method which enables non-destructive analyses due to the dynamic characteristic of caries itself. The high correlation existed between the micro-CT system and the most reliable method of caries analyses stimulates the interest to persist the effort for the validation of the system.

New research should be encouraged to evaluate the equipment for the studies of enamel abrasion and artificial caries in enamel and dentin. Moreover, real time experiments and three-

dimensional analysis of mineral loss could be done as also morphological insight of the development of caries. Longer term experiments could be also stimulated using the most tempting advantage of the method, which is the possibility of conducting longitudinal studies without destroying the samples.

# Zusammenfassung

In den letzten Jahren wurden die Methoden zur Kariesdiagnose und -quantifizierung verbessert. Die Suche nach einer nichtdestruktiven Methode hat das Interesse auf das Micro-CT (Mikro-Computer Tomographie) gelenkt, um Schmelz De/Remineralizierung zu untersuchen. Unser Beitrag zu dieser Entwicklung wurde in dieser Arbeit dargestellt. Wir werteten die Methode hinsichtlich der benötigte Energie und der Größe der Proben aus; außerdem wurden die Ergebnisse vom Mikro-CT zum Mineralverlust- und zur Läsionstiefe mit einer bewährten Methode (Transverse Mikroradiographie - TMR) korrelierten. Anhand diese Daten leiteten wir ein dreidimensionales Modell für die Studie der Dentinkariesexkavation vor.

Nach einer Literaturübersicht im ersten und zweiten Kapitel dieser Arbeit, werteten wir ein kommerzielles *fan-beam* Micro-CT (µCT 20, SCANCO Medical AG, Bassersdorf, Schweiz) der zweiten Generationen für Mineralgehaltmessungen aus. Entsprechend unserer Ergebnisse, ist das Gerät, das bei 50 kVp und 160 µA arbeitet, nicht geeignet, den Mineralgehalt eines vollständigen Zahnes quantitativ zu bestimmen. So empfehlen wir, die begrenzte Nachbeschleunigungsspannung des µCT 20 Systems zu beachten und Auswertungen auf Proben mit 6-Millimeter Querschnitt zu begrenzen. Dies hat gegenüber anderen analytischen Methoden bereits den Vorteil nondestruktiv ohne die sehr dünnen mikrometrischen Proben arbeiten zu können.

Die Korrelation von Mikro-CT und von TMR Ergebnissen wurde in unserem zweiten Experiment ausgewertet (siehe Kapitel 5). Nachdem 70-90 µm dicke Scheiben mit natürlicher Schmelzkaries durch eine TMR analysiert worden sind, wurden Mikro-CT (µCT 40; Scanco

Medical AG, Bassersdorf, Schweiz) Messungen durchgeführt. Die Proben wurden in einen vollständigen Zahnes eingesetzt, der besonders vorbereitet worden war, um eine zerstörungsfreie Auswertung zu simulieren. Auch der Randeffekt wurde ausgewertet, indem man unterschiedliche Schwellen für den Anfang der Läsion verwendete. Unsere Beobachtung zeigte eine hohe Pearson-Korrelation zwischen den Methoden zur Auswertung des Mineralverlustes und Läsionstiefe. Daten unterstützen die Entscheidung erst den Wert von 20 vol% für den Anfang der Läsion zu wählen. Ein höherer Wert scheint nicht notwendig zu sein. Kleinerer Werte können zu einer höheren Veränderung der Werte führen, was auf den Einflusses des Operateurs und dadurch bedürften Artefakten zurückzuführen ist.

In Bezug auf die Dentinexkavation hat sich der Mikro-CT als ein wertvolles Werkzeug erwiesen, um zwischen den drei Phasen der Mineralisierung im kariösen Prozess zu unterscheiden: ein sehr stark entmineralisierter Dentinbereich, eine Schicht zunehmende Mineralisierung und gesundes Dentin. In diesem Kapitel haben wir eine neue Enzymlösung (SFC-V, 3M ESPE AG, Seefeld, Deutschland) für die Behandlung von Dentinkaries mit einer gut belegten Methode verglichen (Carisolv Gel Multimix; MediTeam Dental AB, Gothenburg, Schweden). Der Gebrauch eines Schwellwerts basieren Auswertung zur Differenzierung des entfernten und restlichen Dentins nach Dentinkariesexkavation war sehr vielversprechend. Das mathematische Modell konnte die verbliebene Dicke des entmineralisierten Dentins sehr gut vergleichen und zusätzlich einen Einblick in seine dreidimensionale Perspektive geben.

In dieser Arbeit versuchten wir, die gegenwärtigen Möglichkeiten der Mikro-CT Aufnahmen und Quantifizierung für den Gebrauch in der Kariesforschung zu demonstrieren. Das System hat Beschränkungen ausichtlich der Wahl der Energieintensität, Artefakte während des

Einscannens, der Kalibrierung und der Kosten. Jedoch ist es in der Kariesforschung aufgrund der dynamischen Eigenschaft der Karies erforderlich zerstörungsfreie Analysen vornehmen zu können. Die hohe Korrelation, die zwischen dem Mikro-CT System und der zuverlässigsten Methode der Kariesanalysen (TMR) bestand, bestärkt das Interesse an, mit der Validierung des Systems weiterzumachen.

Das Mikro-CT kann auch für die Studien zur Schmelz Abrasion und künstlichen Karies in Schmelz und Dentin verwendet werden. Außerdem könnten Realzeitexperimente und dreidimensionale Analysen des Mineralverlustes wie auch ein morphologischer Einblick der Entwicklung von Karies durchgeführt werden. Mit dem längerfristige Experimente reizvoll Vorteil longitudinale Studien, ohne die Proben zerstören zu müssen, sind ebenfalls denkbar und möglich.

# References

Akimoto N, Yokoyama G, Ohmori K, Suzuki S, Kohno A, Cox CF (2001). Remineralization across the resin-dentin interface: In vivo evaluation with nanoindentation measurements, EDS, and SEM. *Quintessence Int* 32(7):561-570.

Anderson P, Elliott JC, Bose U, Jones SJ (1996). A comparison of the mineral content of enamel and dentine in human premolars and enamel pearls measured by X-ray microtomography. *Arch Oral Biol* 41(3):281-290.

Angmar B, Glas JE, Carlstrom D (1963). Studies on Ultrastructure of Dental Enamel .4. Mineralization of Normal Human Enamel. *J Ultra Mol Struct R* 8(1):12-23.

Arends J, ten Bosch JJ (1992). Demineralization and remineralization evaluation techniques. *J Dent Res* 71(Spec Issue):924-928.

Axelsson C, Danielsson P (1994). Three-dimensional reconstruction from cone-beam data in O(N3logN) time. *Phys Med Biol* 39:477-491.

Azrak B, Callaway A, Grundheber A, Stender E, Willershausen B (2004). Comparison of the efficacy of chemomechanical caries removal (Carisolv) with that of conventional excavation in reducing the cariogenic flora. *Int J Paediatr Dent* 14(3):182-191.

Beeley JA, Yip HK, Stevenson AG (2000). Chemochemical caries removal: a review of the techniques and latest developments. *Br Dent J* 188(8):427-430.

Berger MJH, J.H.; Seltzer, S.M.; Coursey, J.S.; Zucker, D.S. (1999). XCOM: Photon Cross Section Database (version1.2). National Institute of Standards and Technology, Gaithersburg, MD. Available: http://physics.nist.gov/xcom.

Bergman G, Lind PO (1966). A Quantitative Microradiographic Study of Incipient Enamel Caries. *J Dent Res* 45(5P2):1477-1484.

Bergmans L, Van Cleynenbreugel J, Wevers M, Lambrechts P (2001). A methodology for quantitative evaluation of root canal instrumentation using microcomputed tomography. *Int Endod J* 34(5):390-398.

Bjorndal L, Larsen T, Thylstrup A (1997). A clinical and microbiological study of deep carious lesions during stepwise excavation using long treatment intervals. *Caries Res* 31(6):411-417.

Bjorndal L, Thylstrup A (1998). A practice-based study on stepwise excavation of deep carious lesions in permanent teeth: a 1-year follow-up study. *Community Dent Oral Epidemiol* 26(2):122-128.

Bjorndal L, Larsen T (2000). Changes in the cultivable flora in deep carious lesions following a stepwise excavation procedure. 34(6):502-508.

Bonse U, Busch F (1996). X-ray computed microtomography ($\mu$CT) using synchrotron radiation (SR). *Prog Biophys Mol Bio* 65(1-2):133-169.

Brooks RA, Dichiro G (1976). Beam Hardening in X-Ray Reconstructive Tomography. *Phys Med Biol* 21(3):390-398.

Bushberg JT (1994). Essential Physics of Medical Imaging. 2nd ed.: Williams & Wilkins.

Carlsson CA (1999). Imaging modalities in x-ray computerized tomography and in selected volume tomography. *Phys Med Biol* 44:R23-R56.

Casteele EVd (2004). Model-based approach for Beam Hardening Correction and Resolution Measurements in Microtomography (Dissertation). Antwerpen, University of Antwerpen.

Cloetens P, Boller E, Wolfgang L, Baruchel J, Schlenker M (2001). Absorption and phase imaging with synchrotron radiation. *Europhysics News* 32(2).

Cloetens P, Baruchel J (2002). Synchrotron-radiation Microtomography. European Synchrotron Radiation Facility. Available: http://www.esrf.fr/UsersAndScience/Publications/Highlights/2002/Imaging/IMA1/.

Daculsi G, Kerebel B, Lecabellec MT, Kerebel LM (1979). Qualitative and Quantitative Data on Arrested Caries in Dentin. *Caries Res* 13(4):190-202.

Damen J, Exterkate R, ten Cate J (1997). Reproducibility of TMR for the determination of longitudinal mineral changes in dental hard tissues. *Adv Dent Res* 11(4):415-419.

Davis GR, Wong FSL (1996). X-ray microtomography of bones and teeth. *Physiol Meas* 17(3):121-146.

Davis GR, Elliott JC (1997). X-ray microtomography scanner using time-delay integration for elimination of ring artefacts in the reconstructed image. *Nucl Instr and Meth in Phys Res A* 394(1-2):157-162.

Davis GR (1998). Faster tomographic fan-beam back-projection using Cartesian axes pre-projection. *Nucl Instr and Meth in Phys Res A* 410:329-334.

de Josselin de Jong E, ten Bosch JJ, Noordmans J (1987). Optimised microcomputer-guided quantitative microradiography on dental mineralised tissue slices. *Phys Med Biol* 32(7):887-899.

Dowker SEP, Davis GR, Elliott JC (1997). X-ray microtomography - Nondestructive three-dimensional imaging for in vitro endodontic studies. *Oral Surg Oral Med O* 83(4):510-516.

Dowker SEP, Anderson P, Elliott JC, Gao XJ (1999). Crystal chemistry and dissolution of calcium phosphate in dental enamel. *Mineral Mag* 63(6):791-800.

Dowker SEP, Elliott JC, Davis GR, Wassif HS (2003). Longitudinal study of the three-dimensional development of subsurface enamel lesions during in vitro demineralisation. *Caries Res* 37(4):237-245.

Dowker SEP, Elliott JC, Davis GR, Wilson RM, Cloetens P (2004). Synchrotron x-ray microtomographic investigation of mineral concentrations at micrometre scale in sound and carious enamel. *Caries Res* 38(6):514-522.

Elhila H, Zolfaghari A, Cazaux J, Audran JC, Mouze D (1996). X-ray microscopy and microtomography: Application in biology. *J Phys IV* 6(C4):739-745.

The Encyclopaedia of Medical Imaging. Vol 1, Physics, Techniques and Procedures (1999). In: Radiology. H Pettersson, D Allison, GK von Schulthess and H-J Smith editors.

Endo M, Tsunoo T, Nakamori N, Yoshida K (2001). Effect of scattered radiation on image noise in cone beam CT. *Med Phys* 28(4):469-474.

Fearne J, Anderson P, Davis GR (2004). 3D X-ray microscopic study of the extent of variations in enamel density in first permanent molars with idiopathic enamel hypomineralisation. *Brit Dent J* 196(10):634-638.

Fluckiger L, Waltimo T, Stich H, Lussi A (2005). Comparison of chemomechanical caries removal using Carisolv or conventional hand excavation in deciduous teeth in vitro. *J Dent* 33(2):87-90.

Frank RM, Wolff F, Gutmann B (1964). Microscopie electronique de la carie au niveau de l'email humain. *Arch Oral Biol* 9(2):181-188.

Gao XJ, Elliott JC, Anderson P, Davis GR (1993). Scanning Microradiographic and Microtomographic Studies of Remineralization of Subsurface Enamel Lesions. *J Chem Soc Faraday T* 89(15):2907-2912.

Garberoglio R, Brannstrom M (1976). Scanning Electron-Microscopic Investigation of Human Dentinal Tubules. *Arch Oral Biol* 21(6):355-362.

Gelhard TB, Arends J (1984). Microradiography of in vivo remineralized lesions in human enamel. II. *J Biol Buccale* 12(1):59-65.

Goldman M, Kronman JH (1976). A preliminary report on a chemomechanical means of removing caries. *J Am Dent Assoc* 93(6):1149-1153.

Habib CM, Kronman J, Goldman M (1975). A chemical evaluation of collagen and hydroxyproline after treatment with GK-101 (N-chloroglycine). *Pharmacol Ther Dent* 2(3-4):209-215.

Hafstrom-Bjorkman U, Sundstrom F, de Josselin de Jong E, Oliveby A, Angmar-Mansson B (1992). Comparison of laser fluorescence and longitudinal microradiography for quantitative assessment of in vitro enamel caries. *Caries Res* 26(4):241-247.

Hahn SK, Kim JW, Lee SH, Kim CC, Hahn SH, Jang KT (2004). Microcomputed tomographic assessment of chemomechanical caries removal. *Caries Res* 38(1):75-78.

Hayakawa T, Mishima H, Yokota I, Sakae T, Kozawa Y, Nemoto K (2000). Application of high resolution microfocus X-ray CT for the observation of human tooth. *Dent Mater J* 19(1):87-95.

Herkstroter FM, Noordmans J, Ten Bosch JJ (1990). Wavelength-independent microradiography used for quantification of mineral changes in thin enamel and dentin samples with natural surfaces, pseudo-thick tooth sections, and whole teeth. *J Dent Res* 69(12):1824-1827.

Hildebrand T, Ruegsegger P (1997). A new method for the model-independent assessment of thickness in three-dimensional images. *J Microsc-Oxford* 185(1):67-75.

Hsieh J, Molthen RC, Dawson CA, Johnson RH (2000). An iterative approach to the beam hardening correction in cone beam CT. *Med Phys* 27(1):23-29.

Hunter AR, Treasure ET, Hunter AJ (1995). Increases in Cavity Volume Associated with the Removal of Class-2 Amalgam and Composite Restorations. *Oper Dent* 20(1):2-6.

Huysmans MC, Longbottom C (2004). The challenges of validating diagnostic methods and selecting appropriate gold standards. *J Dent Res* 83(Spec Issue C):C48-52.

International Tables for crystallography. Vol. III (1962). Birmingham: The Kynoch Press.

Itoh M, Shimazu A, Hirata I, Yoshida Y, Shintani H, Okazaki M (2004). Characterization of CO(3)Ap-collagen sponges using x-ray high-resolution microtomography. *Biomat* 25(13):2577-2583.

Johansen E, Parks HF (1961). Electron-Microscopic Observations on Soft Carious Human Dentin. *J Dent Res* 40(2):235-248.

Kak AC, Slaney M (1988). Principles of Computerized Tomographic Imaging. New York: The Institute of Electrical and Electronics Engineers, Inc.

Kalukin AR, Van Geet M, Swennen R (2000). Principal components analysis of multienergy X-ray computed tomography of mineral samples. *Ieee T Nucl Sci* 47(5):1729-1736.

Kato S, Fusayama T (1970). Recalcification of Artificially Decalcified Dentin in-Vivo. *J Dent Res* 49(5):1060-1067.

Ketcham RA, Carlson WD (2001). Acquisition, optimization and interpretation of X-ray computed tomographic imagery: applications to the geosciences. *Computers & Geosciences* 27(4):381-400.

Kidd EAM, Joystonbechal S, Beighton D (1993). The Use of a Caries Detector Dye During Cavity Preparation - a Microbiological Assessment. *Brit Dent J* 174(7):245-248.

Kidd EAM (2004). How 'clean' must a cavity be before restoration? *Caries Res* 38(3):305-313.

Klont B, ten Cate JM (1990). Release of organic matrix components from bovine incisor roots during in vitro lesion formation. *J Dent Res* 69(3):896-900.

Kronman JH, Goldman M, Habib CM, Mengel L (1977). Electron-Microscopic Evaluation of Altered Collagen Structure Induced by N-Monochloroglycine (Gk-101). *J Dent Res* 56(12):1539-1545.

Kuboki Y, Ohgushi K, Fusayama T (1977). Collagen Biochemistry of 2 Layers of Carious Dentin. *J Dent Res* 56(10):1233-1237.

Kuboki Y (1991). Preparation of collagen from hard tissue. In: Collagen experimental method. Y Nagai and D Fujimoto editors. Tokyo: Kodansha, pp. 21-30.

Lager A, Thornqvist E, Ericson D (2003). Cultivatable bacteria in dentine after caries excavation using rose-bur or Carisolv. *Caries Res* 37(3):206-211.

Landis E, Keane D, Shah L Microtomography of Cement-Based Materials. National Science Foundation. Available: http://www.umeciv.maine.edu/landis/XMT/Default.htm.

Levine RS, Rowles SL (1973). Further studies on the remineralization of human carious dentine in vitro. *Arch Oral Biol* 18(11):1351-1356.

Lin CL, Miller JD (1996). Cone beam X-ray microtomography for three-dimensional liberation analysis in the 21st century. *Int J Miner Process* 47(1-2):61-73.

Lindblom K (1954). On microtomography. *Acta Radiol* 42(6):465-468.

Mellberg JR, Chomicki WG, Mallon DE, Castrovince LA (1985). Remineralization Invivo of Artificial Caries Lesions by a Monofluorophosphate Dentifrice. *Caries Res* 19(2):126-135.

Mercer CE, Anderson P, Davis GR (2003). Sequential 3D X-ray microtomographic measurement of enamel and dentine ablation by an Er : YAG laser. *Brit Dent J* 194(2):99-104.

Miller EJ, Rhodes RK (1982). Preparation and Characterization of the Different Types of Collagen. *Methods Enzymol* 82:33-64.

Morton EJ, Webb S, Bateman JE, Clarke LJ, Shelton CG (1990). 3-Dimensional X-Ray Microtomography for Medical and Biological Applications. *Phys Med Biol* 35(7):805-820.

Nuzzo S, Peyrin F, Cloetens P, Baruchel J (2002). Quantification of the degree of mineralization of bone in three dimensions using synchrotron radiation microtomography. *Med Phys* 29(11):2672-2681.

Ohgushi K, Fusayama T (1975). Electron-Microscopic Structure of 2 Layers of Carious Dentin. *J Dent Res* 54(5):1019-1026.

Oi T, Saka H, Ide Y (2004). Three-dimensional observation of pulp cavities in the maxillary first premolar tooth using micro-CT. *Int Endod J* 37(1):46-51.

Pashley EL, Talman R, Horner JA, Pashley DH (1991). Permeability of Normal Versus Carious Dentin. *Endodontics & Dental Traumatology* 7(5):207-211.

Pearisamy K, Anderson P (2000). Scanning microradiographic monitoring of enamel remineralisation following etch and pumicing. *J Dent Res* 79(5):1206-1206.

Perdigao J, Lambrechts P, Vanherle G (1995). A Morphological Field-Emission Sem Study of Acid-Etched Dentin. *J Dent Res*
*J Dent Res* 74(3):916-916.

Peters OA, Peters CI, Schonenberger K, Barbakow F (2003). ProTaper rotary root canal preparation: effects of canal anatomy on final shape analysed by micro CT. *Int Endod J* 36(2):86-92.

Pettersson H, Allison D, von Schulthess GK, Smith H-J (1998). The Encyclopaedia of Medical Imaging: NICER Institute/ISIS Medical Media.

Rhodes JS, Ford TRP, Lynch JA, Liepins PJ, Curtis RV (1999). Micro-computed tomography: a new tool for experimental endodontology. *Int Endod J* 32(3):165-170.

Rhodes JS, Ford TRP, Lynch JA, Curtis RV (2000). A comparison of two nickel-titanium instrumentation techniques in teeth using microcomputed tomography. *Int Endod J* 33(3):279-285.

Robinson C, Weatherell JA, Hallsworth AS (1971). Variatoon in composition of dental enamel within thin ground tooth sections. *Caries Res* 5(1):44-57.

Rossi M, Casali F, Romani D, Bondioli L, Macchiarelli R, Rook L (2004). MicroCT Scan in paleobiology: application to the study of dental tissues. *Nucl Instrum Meth B* 213:747-750.

Salome M, Peyrin F, Cloetens P, Odet C, Laval-Jeantet AM, Baruchel J, Spanne P (1999). A synchrotron radiation microtomography system for the analysis of trabecular bone samples. *Med Phys* 26(10):2194-2204.

Sato Y, Fusayama T (1976). Removal of Dentin by Fuchsin Staining. *J Dent Res* 55(4):678-683.

Schutzbank SG, Galaini J, Kronman JH, Goldman M, Clark RE (1978). Comparative Invitro Study of Gk-101 and Gk-101e in Caries Removal. *J Dent Res* 57(9-10):861-864.

Selvig KA (1968). Ultrastructural changes in human dentine exposed to a weak acid. *Arch Oral Biol* 13(7):719-726.

Sohmura T, Wakabayashi K, Lowmunkong R, Hojo H, Kusumoto N, Okuda H, Kojima T, Nakamura T, Yatani H, Takahashi J (2004). 3D shape measurement of dental casts using medical X-ray CT. *Dent Mater J* 23(2):121-128.

Sokolik IN (2005). Basic radiometric quantities. The Beer-Bouguer-Lambert law. Concepts of extinction (scattering plus absorption) and emission. Schwarzschild's equation. Available: http://irina.eas.gatech.edu/EAS8803Fall2005/Lecture3.pdf.

Spanne P (1989). X-Ray-Energy Optimization in Computed Microtomography. *Phys Med Biol* 34(6):679-690.

Stock SR, Barss J, Dahl T, Veis A, Almer JD (2002). X-ray absorption microtomography (microCT) and small beam diffraction mapping of sea urchin teeth. *J Struct Biol* 139(1):1-12.

Takeda T, Itai Y, Hayashi K, Nagata Y, Yamaji H, Hyodo K (1994). High spatial resolution CT with a synchrotron radiation system. *J Comput Assist Tomogr* 18(1):98-101.

ten Bosch JJ, Angmar-Mansson B (1991). A Review of Quantitative Methods for Studies of Mineral-Content of Intraoral Incipient Caries Lesions. *J Dent Res* 70(1):2-14.

Theuns HM, Driessens FC, van Dijk JW, Groeneveld A (1986). Experimental evidence for a gradient in the solubility and in the rate of dissolution of human enamel. *Caries Res* 20(1):24-31.

Tonami KI, Araki K, Mataki S, Kurosaki N (2003). Effects of chloramines and sodium hypochlorite on carious dentin. *J Med Dent Sci* 50(2):139-146.

Tonami KI, Ericson D (2005). Protein profile of pepsin-digested carious and sound human dentine. *Acta Odontol Scand* 63(1):17-20.

Tveit AB, Selvig KA (1981). Invivo Re-Calcification of Dentin Demineralized by Citric-Acid. *Scandinavian J Dent Res* 89(1):38-42.

Tyas MJ, Anusavice KJ, Frencken JE, Mount GJ (2000). Minimal intervention dentistry - a review - FDI Commission Project 1-97. *Int Dent J* 50(1):1-12.

Van Geet M (1997). X-Ray Microfocus Computer Tomography. Katholieke Universiteit Leuven. Available: http://www.kuleuven.be/geology/Fcg/Sediment/Research/maarten/xray.htm.

Wakabayashi K, Sohmura T, Nakamura T, Kojima T, Kinuta S, Takahashi J, Yatani H (2005). New evaluation method by microfocus radiograph CT for 3D assessment of internal adaptation of all-ceramic crowns. *Dent Mater J* 24(3):362-367.

Weatherell JA, Weidmann SM (1967). Density Patterns in Enamel. *Caries Res* 1:42-51.

Wilson PR, Beynon AD (1989). Mineralization Differences between Human Deciduous and Permanent Enamel Measured by Quantitative Microradiography. *Arch Oral Biol* 34(2):85-88.

Wolfgang L (2001). Development and applications of synchrotron radiation microscopy (Dissertation). München, Ludwig-Maximilians-Universität München.

Wong FS, Elliott JC, Anderson P, Davis GR (1995). Mineral concentration gradients in rat femoral diaphyses measured by X-ray microtomography. *Calcif Tissue Int* 56(1):62-70.

Wong FS, Elliott JC, Davis GR, Anderson P (2000). X-ray microtomographic study of mineral distribution in enamel of mandibular rat incisors. *J Anat* 196(Pt 3):405-413.

Wong FSL, Anderson P, Fan H, Davis GR (2004). X-ray microtomographic study of mineral concentration distribution in deciduous enamel. *Arch Oral Biol* 49(11):937-944.

Yip HK, Stevenson AG, Beeley JA (1994). The Specificity of Caries Detector Dyes in Cavity Preparation. *Brit Dent J* 176(11):417-421.

Yip HK, Beeley JA, Stevenson AG (1995). Mineral content of the dentine remaining after chemomechanical caries removal. *Caries Res* 29(2):111-117.

Young RA, Brown WE (1982). Structures of biological minerais. In: Nacollas Biological mineralization and demineralization. Dahlem Konferenzen. Berlim: Springer Verlag, pp. 101-141.

Young S, Muller H, Marshall W (1983). Computed tomography: beam hardening and environmental density artifact. *Radiology* 148(1):279-283.

Zolfaghari A (1996). An iterative reconstruction algorithm in cone beam geometry: Simulation and application in X-ray microtomography. *Nucl Instrum Meth A* 378(1-2):326-336.

# Acknowledgments

The plan and elaboration of this dissertation could only be rendered with the supportive interest, encouragement and tangible contribution of many people. Therefore, I have the privilege to acknowledge the assistance of all who participate in the preparation of this thesis.

Agradeço primeiramente ao meu marido Gustavo Luedemann, que me encorajou a seguir meu coração e buscar meus sonhos. Pelo seu apoio, nos momentos de dúvida e desânimo, sempre me estimulando a pensar de forma científica e racional. Também pelo seu amor que me fez suportar a distância da minha terra querida. Agradeço a meu filho, João Pedro, que ainda na minha barriga, sem ter conhecimento, encheu-me de força para concluir minha pesquisa e finalizar este trabalho. Eu os amo demais!

Minha amada família, papai, mamãe, Tatá, Marcelo e Nanana. Por mais uma vez apoiar minha partida em busca dos meus sonhos. Tenho certeza que sem o amor presente de vocês a distância e o caminho seriam mais duros. Meu eterno MUITO OBRIGADA!!!

An meinen Doktorvater Prof. Dr. Karl-Heinz Kunzelmann mein herzlichen Dank für sein Vertrauen und seine Unterstützung. Seine Kompetenz und Bereitwilligkeit neue Anwendungen für das Mikro-CT in der zahnmedizinischen Forschung zu entdecken ergaben eine fruchtbare und dauernde Zusammenarbeit.

I would like to thank the Director of the Department of Restorative Dentistry of the University of Munich, Prof. Dr. Reinhard Hickel, for the encouragement and support to send me to all important scientific congresses which took place during my stay. It was exactly in one of these conferences that I had the privilege to meet Dr. Jaap ten Bosch. I am very grateful to you, Jaap, for all helpful discussion concerning the planning of this work, insuring that even with the distance, every small detail would be properly done. Thanks for trusting on me and on this project.

106

# Curriculum Vitae

**Name:** Tatiana Nogueira Rocha Clementino Luedemann

**Place and date of birth:** Brasília, DF, Brazil – 04.12.1976

**Civil status:** Married

**Primary School:**

Escola Paroquial Santo Antônio (1984 – 1990). Brasília, DF, Brazil

Centro Educacional Sigma (1991). Brasília, DF, Brazil

**Secondary School:**

Colégio Objetivo (1992). Brasília, DF, Brazil

North Carolina School of Arts (1992 – 1993), Winston Salem, USA

Colégio Objetivo (1994 – 1995). Brasília, DF, Brazil

**Undergraduation:**

Pontifícia Universidade Católica (1996 – 2000). Belo Horizonte, MG, Brazil – Degree of Dental Science

**Post-graduation:**

Escola de Aperfeiçoamento Profissional – ABO/MG. Belo Horizonte, MG, Brazil – Especialization in Restorative Dentistry

**Publications:**

Clementino-Luedemann, T. N. R and Kunzelmann, K-. H (2006). Mineral Concentration of Natural Human Teeth by a Commercial Micro-CT. *Dent Mater J* 25(1)*:*113-119.

Clementino-Luedemann, T. N. R; Dabanoglu, A.; Ilie, N; Hickel, R. and Kunzelmann, K-. H. (2006). Micro-computed Tomographic Evaluation of a New Enzyme Solution for Caries Removal in Deciduous Teeth. *Dent Mater J* 25(4)*:*675-683.